Post Access Report

Pterofin Skimmer

Awardee: Pterofin

Awardee point of contact: Wallace Kempkey

Facility: Applied Research Laboratory, Pennsylvania State University

Facility point of contact: Dr. Nicholas Jaffa

Facility test report authors: Dr. Nicholas Jaffa, Justin Walsh, Jon Bechtel, Dr. Alexander Piqué, Tim Durachko

Date: 10/27/2023

EXECUTIVE SUMMARY

Pterofin has utilized bio-mimicry to replicate the forces of propulsion demonstrated by many species of aquatic life within the animal kingdom, which can be reverse engineered to create hydroelectricity without impacting the surrounding environment. Because it takes time for a Stokes-type boundary layer to separate, large non-steady effects are anticipated in the limit of large reduced frequency, allowing for potentially greater energy production than a traditional turbine. Pterofin has hypothesized that this flow regime offers engineering benefits compared with traditional hydrokinetic turbine technologies. The complex nature of these flows indicated

the utility of conducting exploratory testing of canonical compound flapping/pitching hydrofoils to guide development of these technologies.

1 Introduction to the Project

Pterofin's Skimmer concept (Figure 1) relies on a flapping and pitching hydrofoil to extract hydrokinetic energy from water flows. The concept aims to utilize unsteady fluid dynamics phenomena (added mass, shed vorticity, and unsteady boundary layer development) to achieve higher lift coefficients, enabling increased power density of the hydrokinetic device and a fundamental shift in the rpm/torque scaling of the power take off compared with turbines. It should be noted that the current Skimmer system is a proof of concept demonstrator, not a full system prototype. At this early stage of the R&D process, there are no true predictions of the hydrodynamic and mechanical system performance.

Figure 1: Pterofin Skimmer Proof of Concept Demonstrator

Utilizing these highly unsteady fluid effects requires evaluating performance across a wide range of reduced frequencies (up to $k = \frac{\omega c}{V} \leq 1$), which are beyond the typical applicable range of standard analytical or numerical design/analysis tools such as blade element method or steady Reynolds Averaged Navier Stokes (RANS) CFD methods. Canonical unsteady aerodynamics solutions (i.e. Sears Function and Theodorsen Function) do not adequately capture the compound flapping and pitching motion or the integrated 3D effects across the hydrofoil span. The most effective method for analyzing these effects is empirically via testing a flapping/pitching semi-canonical test platform. The empirical dataset resulting from these tests will inform the development of the Skimmer system towards the most advantageous region of the design space. Furthermore, the dataset can be used to assist with predictions of expected performance characteristics at full scale and development of a full prototype system.

2 Roles and Responsibilities of Project Participants

Both ARL and Pterofin have responsibilities.

2.1 Applicant Responsibilities and Tasks Performed

Pterofin's responsibility was to provide guidance on the relevant system key parameters and prioritization. Pterofin was also responsible for building/supplying the hydrofoil/fins to be utilized in the tunnel test in order to be compliant with TEAMER budget restrictions.

2.2 Network Facility Responsibilities and Tasks Performed

ARL's responsibility was to design and build a feasible test platform for studying the flapping pitching hydrofoil concept empirically in ARL's water tunnels. ARL planned and executed the experimental testing with prioritization guidance provided by Pterofin within the schedule/budget constraints. ARL performed initial data processing to ensure validity of the basic performance metrics.

3 Project Objectives

The projects' overall objective was to build up a dataset of hydrodynamic performance across a range of primary design variables:

- Reduced frequency
- Reynolds number
- Ratio of flapping/pitching angle magnitude

The range of the reduced frequency testing was intended to span from the quasi-steady range (k = 0.01) to the fully unsteady range (k = 1). This was done experimentally by varying the motor/generator rpm while holding flowrate constant. The range of Reynolds numbers tested exceeded the turbulent transition range for hydrofoils (minimum of approximately 200,000), with sufficient test cases above this level to verify the data is in the Reynolds in-sensitive flow regime. Reynolds number invariance will aid with future scaling of results and guide development of future prototypes. Reynolds number was varied experimentally by varying the flowrate in the water tunnel. The range of flapping arc length tested was determined during ARL's hydrodynamic and drivetrain scaling and design. Specifically, this was determined by the estimated blockage effects hydrodynamically and the feasible range of gearing/flapping ratios of reasonable sized drivetrain mechanisms. Only one flapping arc length was tested based on cost and schedule constraints imposed by the compound flapping/pitching mechanism. Specifically, adjusting the flapping arc length would require manufacturing an additional cam for the mechanism and would require significant delays to disassemble and then reassemble the entire drivetrain mechanism, which would limit testing. The range of flapping/pitching angle magnitude tested was determined during ARL's hydrodynamic and drivetrain scaling and design. Specifically, this analysis looked at the hydrofoil section local instantaneous angle of attack during the motion as well as relative gearing ratios in the compound flapping/pitching mechanism to determine feasible limits (effectively assuming a quasi-steady approximation). This ratio was varied experimentally by changing the gearing ratio in the compound flapping/pitching mechanism (in this case by switching out pulley sizes connecting the flapping shaft with the pitching shaft).

Within budget and schedule constraints, testing allowed for expansion of secondary design variables to include variations in the hydrofoil chord length or aspect ratio, and sweep angle or pivot location via switching out different hydrofoils on the test article. Overall budget constraints prevented the ARL's larger 48" water tunnel being used for the majority of testing during this TEAMER proposal so the 12" diameter water tunnel was utilized with the circular test section.

The major dependent variables to be measured included:

- Power Coefficient (i.e. efficiency)
- Torque Coefficient

These were calculated from time-series measurements of:

- Shaft angular position
- Torque
- Fluid velocity

The time-series of shaft angular position was used to determine the kinematic position and motion ($\omega = \frac{d\theta}{dt}$) of all parts of the drivetrain and hydrofoil. The power extracted was calculated via the product of the shaft motion and the shaft torque (at the motor/generator). The drivetrain frictional losses were measured via a windage test of the mechanism without the hydrofoil and subtracted off the system measurements to calculate the power coefficient of the hydrofoil only. Since there was no ready method for applying load to the drivetrain during the windage test, the sensitivity of the drivetrain frictional losses to load was not able to be measured and remained a potential source of measurement uncertainty. The fluid freestream velocity and the swept area were used to non-dimensionalize the performance data. The freestream fluid velocity was measured by a pitot-static pressure measurement. At low fluid velocities (i.e. low Reynolds number), the resolution and accuracy of the differential pressure measurement led to increased uncertainty.

The purpose of this database was to guide the development of Pterofin's pitching/flapping hydrofoil technology by pointing towards the regions of the design space that take advantage of the governing physics and provide engineering benefit. Additionally, the testing generated the first real data to quantify the performance potential of a compound flapping/pitching hydrofoil for extracting hydrokinetic power.

4 Test Facility, Equipment, Software, and Technical Expertise

To keep within budget constraints, ARL's 12" diameter water tunnel (shown in Figure 2) was used for testing. This facility is a closed loop water tunnel with a 12" diameter circular test section. The 12" tunnel is capable of a maximum freestream velocity of 21 m/s in the test section and has low inflow turbulence. The tunnel is pressurized for control of cavitation and can be controlled from sub-atmospheric pressure (3 psia) to higher pressure (60 psia). The tunnel contains multiple interchangeable windows for swapping out test apparatus as well as providing optical access for visual monitoring and advanced flow measurements (LDV, PIV, PSV, etc…). Pressure measurements come from existing transducers with a series of ranges (absolute and differential) and can be connected to a range of static pressure taps or pressure probes (pitot, kiel, 5-hole, etc…). Data acquisition systems contain low and high speed DAQ cards and are run on custom Labview software developed in-house.

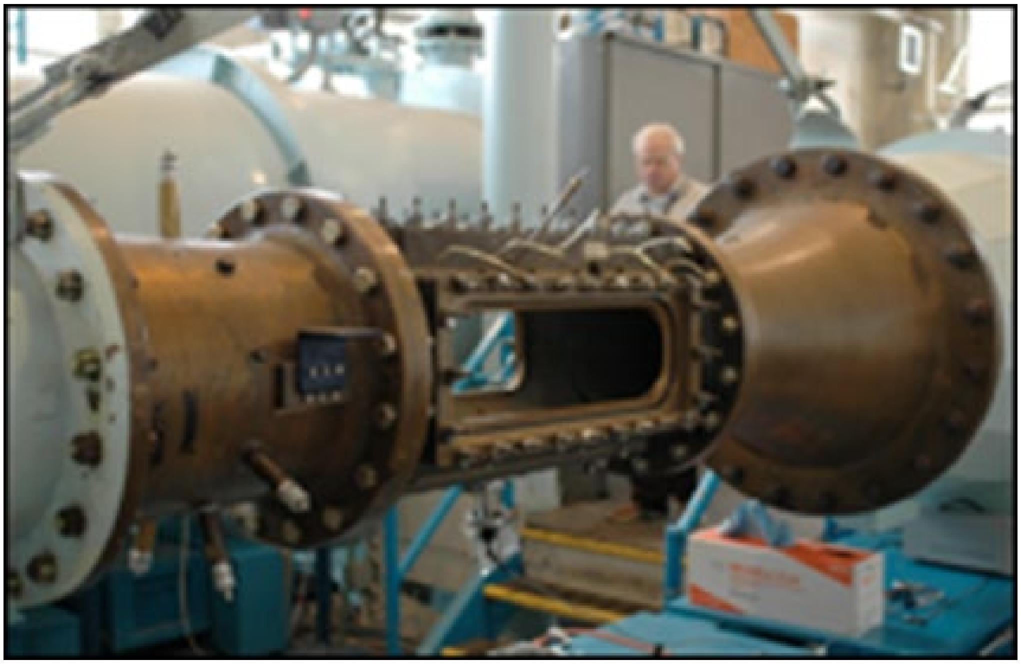

Figure 2: ARL's 12" Water Tunnel shown with Circular Test Section

Shaft torque was measured via a rotary shaft torque sensor. Absolute angular position was measured via a shaft encoder. Windage tests were used to correct the drivetrain frictional losses. Upstream of the hydrofoil, flowrate was measured via a Keil probe and static pressure taps mounted in the tunnel test section. Differential pressure transducers were used to measure the dynamic pressure and thus determine the fluid velocity via Bernoulli's equation.

Critical personnel include subject matter experts in the areas of design and testing of actuated hydrodynamic systems.

- Dr. Nicholas Jaffa
- Mr. Justin Walsh

5 Test or Analysis Article Description

Pterofin's Skimmer concept relies on a pitching/flapping hydrofoil to extract hydrokinetic energy from a water flow. Figure 3 shows an initial qualitative look at the relevant hydrofoil dynamics using a simple quasi-steady approximation from blade element theory.

Oscillating Hydrofoil Dynamics (Initial Qualitative Assessment from Blade Element Theory)

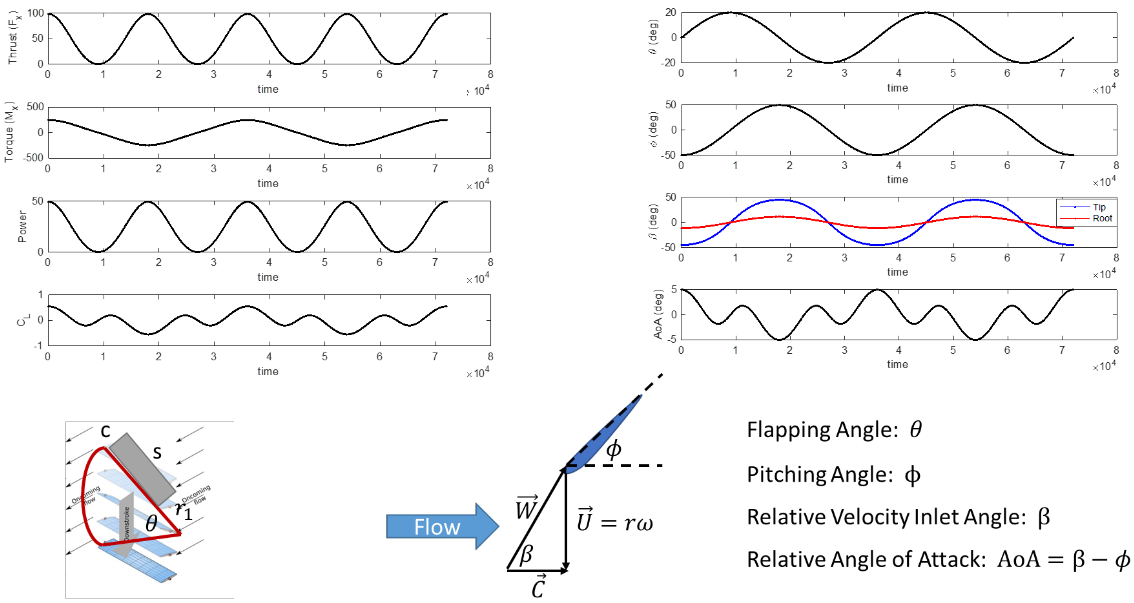

Figure 3: Pitching/Flapping Hydrofoil Dynamics

Pterofin's key argument for the skimmer system having potentially large benefits in terms of system metrics (efficiency, power/weight, cost, etc…) is centered around the system intending to operate at reduced frequencies significantly above the quasi-steady flow regime (where traditional hydrokinetic turbines operate) putting them in parts of the hydrokinetic system design space governed by different and less well understood flow physics (highlighted in Figure 4). The pitching/flapping hydrofoil system, operating at high reduced frequencies, produces a kinematically complex and unsteady flow field. This complex flow field is difficult to predict via analytical or simple numerical methods and justifies an experimental methodology.

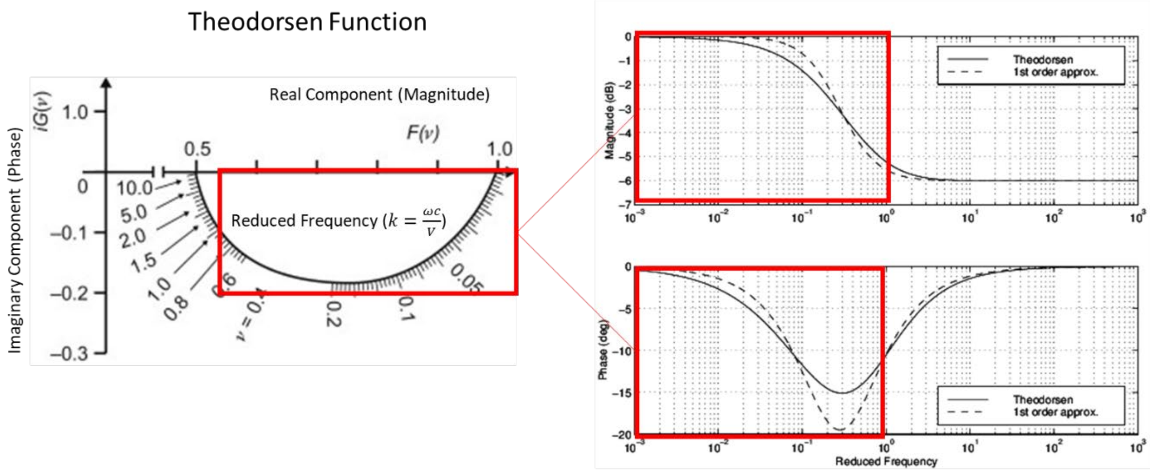

Dominant physics can vary greatly as function of reduced frequency.

1. Steady state aerodynamics – k=0
2. Quasi-steady aerodynamics – 0≤k≤0.05
3. Unsteady aerodynamics – k>0.05 [k>0.2 is considered highly unsteady]

Figure 4: Approximate Unsteady Aero/Hydrodynamic Range

Primary variables of interest from Section 3 are:

- Reduced frequency
- Reynolds number
- Ratio of flapping/pitching angle magnitude

Based on Pterofin's region of interest, the reduced frequency should vary between zero and 1, which can be accomplished by varying the motor/generator rpm for a given tunnel freestream velocity. Reynolds number should be above transition which typically occurs at a chord based Reynolds number of 100,000-200,000. This should be easily achievable since the high maximum tunnel velocity of 21 m/s allows for Reynolds numbers in the millions. Reynolds number can be changed by setting a different tunnel freestream velocity. Flapping and pitching magnitude changes require physical adjustments to the drivetrain mechanisms to alter the kinematic relationships. These were altered by changing the effective gearing ratio.

Secondary variables of interest are:

- Chord or aspect ratio of hydrofoil
- Shape of the hydrofoil planform
- Hydrofoil position and sweep angle relative to pitching axis

Primary unknowns relating the test configuration are:

- Blockage effects

- Free-surface effects
- Load effects on the test article frictional losses

Blockage effects are likely to be present due to the required minimum size of the test assembly relative to the tunnel. These will have to be assumed to be relatively constant bias errors. The can be corrected for in future testing at a larger scale (such as testing the same system in ARL's 48" water tunnel). Free surface effects will need to be ignored since the water tunnel will need to be filled and sealed in order to reach the desired flow velocities. These effects can be assumed to be relatively minor and can be quantified in future testing at a different facility (either ARL's 48" water tunnel or an open channel/tow tank)

6 WORK PLAN

The work plan includes the following activities:

1. Hydrodynamic modeling: Model the system hydrodynamics for the purpose of scaling/sizing as well as informing design of water tunnel test article.
2. Drivetrain modeling: Model the system drivetrain for purpose of scaling/sizing as well as informing design of water tunnel test article.
3. Design tunnel test article: Design system integrated into appropriately sized/scaled experimental test article for water tunnel testing including design of experiment.
4. Build tunnel test article: Build system integrated into experimental test article for water tunnel testing.
5. Water tunnel testing: Setup and execute water tunnel test experiments. Analyze measurements and provide test data on system performance over range of the four desired primary variables of interest (Reynolds number, reduced frequency, pitching amplitude, and flapping amplitude). Secondary variables of interest include the size, shape, and positioning of the fin attached to the mechanism.

Activities 1 and 2 were required in order to determine the test article specifications and testing capabilities. These results were used to inform activity 3, which covers design of the test article and specifies the limits of the ranges. Activity 4 involved building the test article utilizing as much existing ARL components/hardware as feasible within expected operating specifications. Activity 5 involved conducting the experimental investigation and providing the reduced test data. All of the following data and results come out of activity 5.

6.1 Experimental Setup, Data Acquisition System, and Instrumentation

Figure 5 shows the circular test section of ARL's 12-inch water tunnel from the console side. The compound pitching/flapping drivetrain mechanism was mounted on top of the test section. The test section's removable window provided access for model changes.

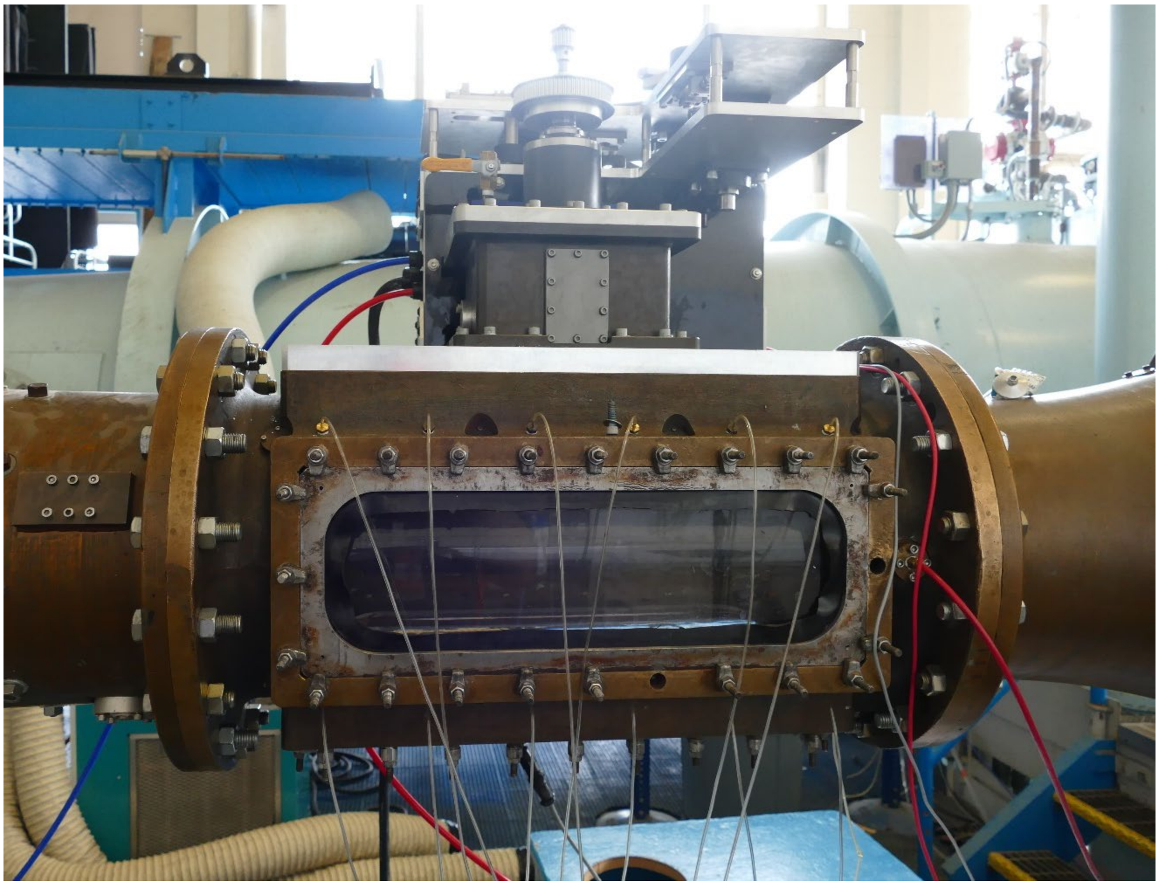

Figure 5: 12-inch water tunnel test section with pitching/flapping mechanism

Figure 6 shows the reverse side of the test section where the 20 hp electric motor was mounted. The pitch mechanism foundation structure above the motor also enclosed the motor connections and shaft instrumentation for safety.

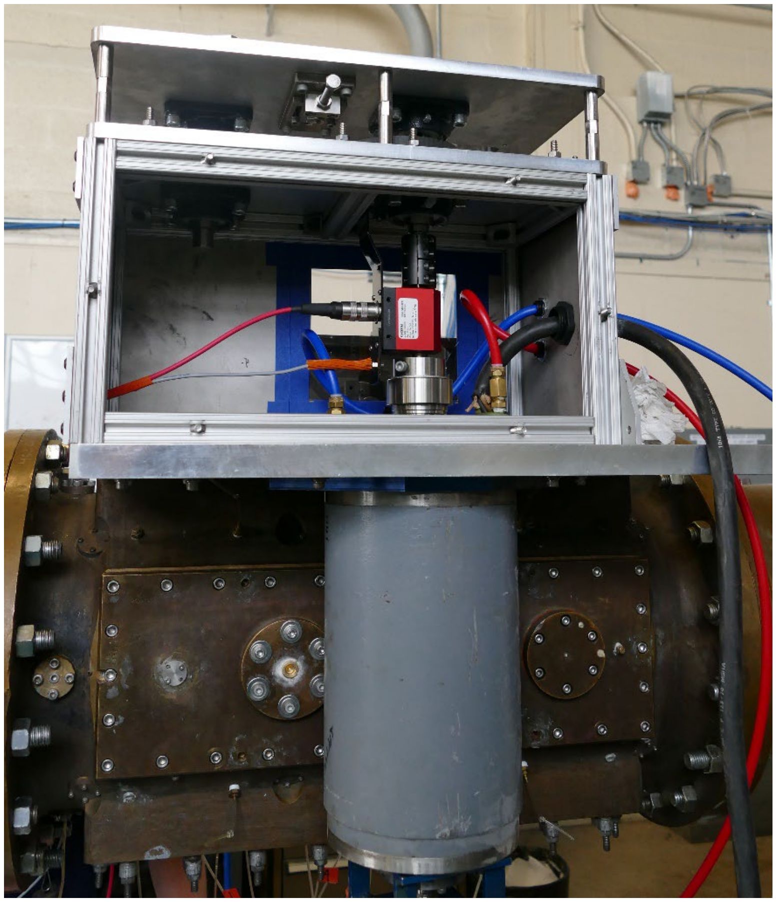

Figure 6: 20hp drive motor, instrumentation and motor connection enclosure.

Figure 7 contains a schematic diagram of the test article and the various constituent mechanisms and sensors. The 20hp electric motor drives two parallel belt drives with 2:1 speed ratios, low backlash, and low stretch.

The upper belt drives the Pitch Mechanism (PM) containing a crank-rocker which is a subtype of the four-bar mechanism. The crank-rocker links (or bars) are dimensioned for unity time ratio [1] such that the forward and reverse strokes both require 180 degrees of PM input shaft rotation. Though the forward and reverse strokes take equal amounts of input shaft rotation (and thus time at constant input shaft speed) the kinematics of the mechanism enforce greater angular acceleration during reversal at one extreme output shaft angular position compared with the other. The PM output shaft oscillates 45 degrees peak to peak with approximately sinusoidal motion once for every two rotations of the motor shaft. A belt drive from the PM output shaft to the pitch shaft enables amplification of the pitch angle through pulley selection.

The lower belt drives the Flapping Mechanism (FM) consisting of a bearing and seal assembly supporting a pair of co-axial shafts, waterproof housing, swashplate, and follower carriage assembly. As the FM input shaft rotates the inclined plane of the attached swashplate drives a follower forcing the flapping carriage to oscillate. The flapping carriage supports the fin as it oscillates in a sinusoidal motion having 45 degree amplitude from peak to peak. Transmission of the pitching motion to the fin through the flapping mechanism required the addition of a single universal joint centered on the flapping axis. 45 degrees was selected as the swept flapping arc for this test because it is the largest angle that the test section can accommodate with the fins tested. Smaller flapping arcs are possible through installation of swashplates with shallower inclined planes, but was not altered during testing due to budget and schedule constraints.

1. Secondary position enc.
2. 20hp electric motor
3. Torque cell and primary position enc.
4. Pitch Mechanism (PM)
5. PM output shaft (+/- 22.5°)
6. Pitch shaft (+/-33.8° to 67.5°)
7. Flapping Mechanism (FM)
8. Pitch universal joint
9. Swashplate and rotating FM shaft
10. Follower and flapping carriage
11. Fin / hydrofoil
12. Timing belt drives

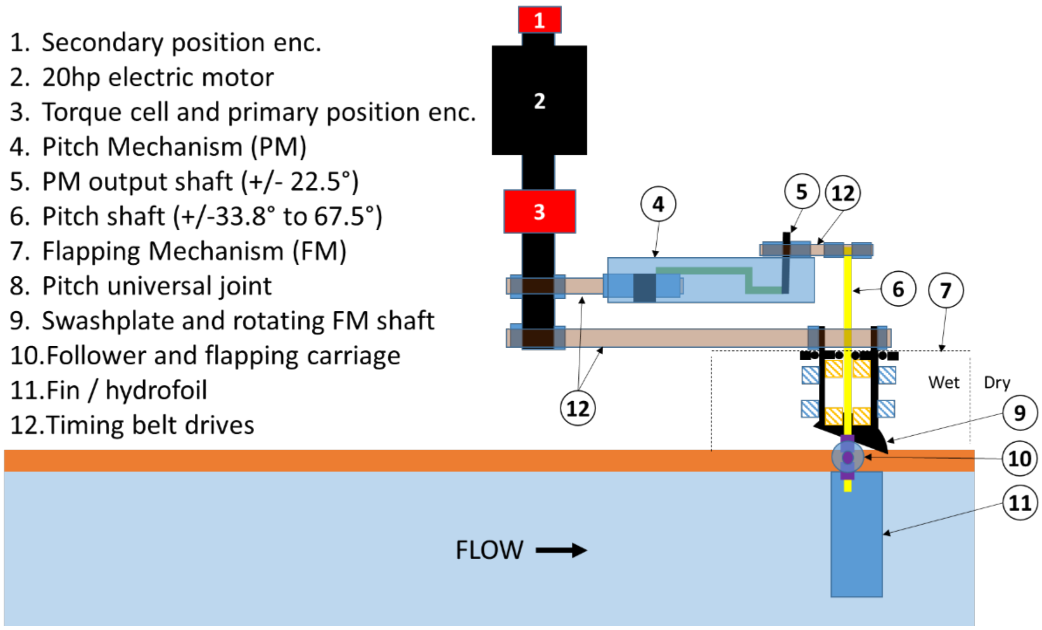

Figure 7: Test article schematic diagram

The hydrofoils/fins provided by Pterofin are shown in Figure 8. The aluminum fins had a maximum span of 6.00 inches, maximum thickness of 0.25 inches, and maximum chord lengths ranging from 1 to 2 inches. Fins A and B featured streamlined cross sections while fins C, D, and E were flat plates. The planform of the fins was predominately rectangular, with fins A and B having tapering trailing and leading edges respectively. Fins A and B featured slotted mounting holes to enable them to be translated or swept relative to the pitching axis of the flapping/pitching mechanism. Fins C, D, and E were mounted to the pitching axis of the flapping/pitching mechanism on their ¼-chord point with no sweep.

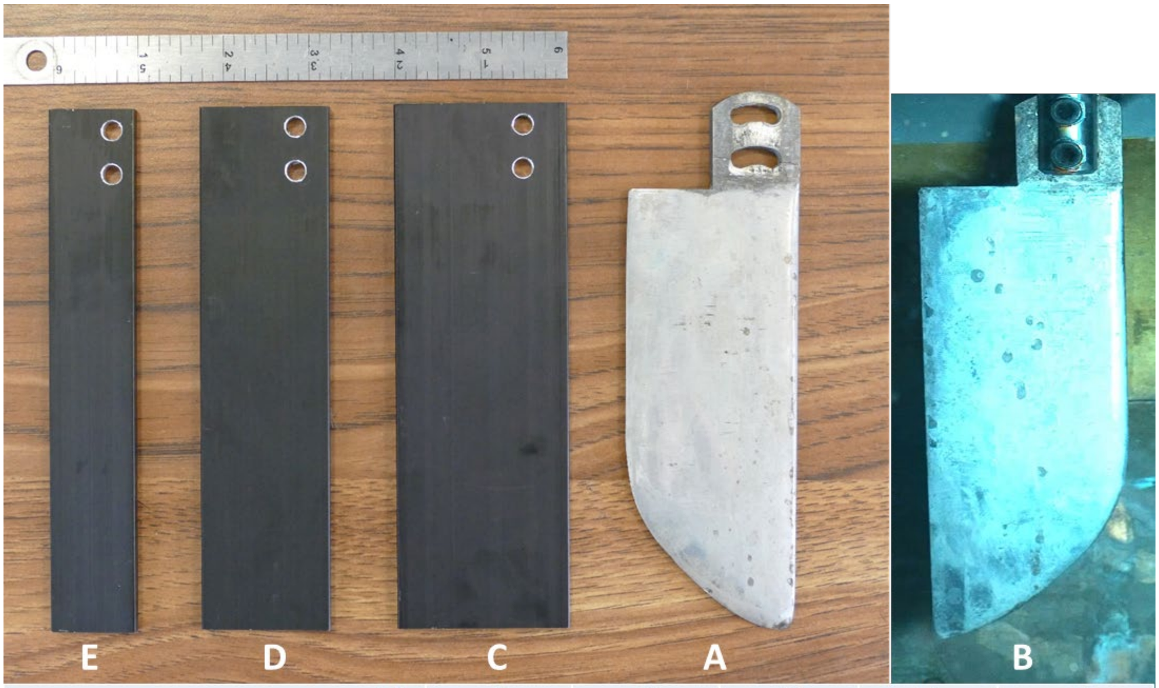

Fin	A	B	C	D	E
Semi-Span (in)	5.00	5.00	6.00	6.00	6.00
Thickness (in)	0.25	0.25	0.25	0.25	0.25
Root Chord (in)	2.00	2.00	2.00	1.50	1.00
Approx Std. Mean Chord (in)	1.84	1.84	2.00	1.50	1.00
t/c	0.14	0.14	0.13	0.17	0.25
Aspect Ratio	5.43	5.43	6.00	8.00	12.0
Approx. Planform Area (in^2)	9.20	9.20	12.0	9.00	6.00

Figure 8: Hydrofoil/fins provided by Pterofin with geometric parameters

ARL utilized an existing 20hp motor/generator and shaft encoder in order to minimize hardware costs. The specifications of the test assembly derived from the hydrodynamic scaling and initial mechanical pitching/flapping mechanism sizing are:

- Flap angle: 45° (+/- 22.5° from vertical)
- Pitch ratio = (pitch angle)/(flap angle): 1.5, 2, 2.5, 3
- Flapping and pitching oscillation frequency: 0.5-10 Hz
- Fin root flap torque: 37 ft-lbf
- Fin pitch torque: 6 ft-lbf
- Frequency ratio, motor shaft to fin: 2

Measurements of primary interest were:

- Motor shaft position
- Motor shaft torque
- Freestream velocity (from total pressure and selected wall static pressures)
- Water temperature

Also measured:

- Wall static pressure in the test section at the locations shown in Figure 9
- High speed video of the for a subset of fin configurations and conditions

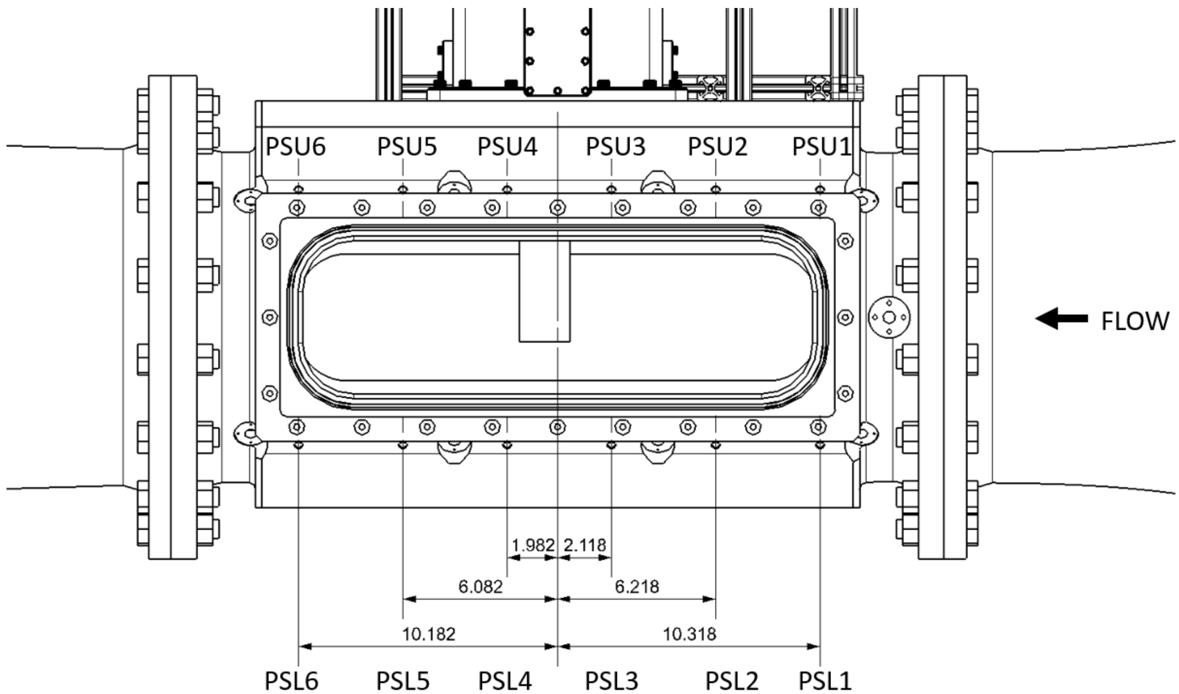

Figure 9: Upper (PSU) and lower (PSL) wall static pressure tap locations on the console side of the test section. Pressure tap locations are shown in inches relative to fin shaft centerline.

Motor shaft torque was measured via a torque sensor mounted between the motor and the flapping/pitching mechanism. The torque sensor incorporated a relative encoder with digital output for measurement of motor shaft position. The calculation of absolute motor shaft position was enabled by a 1 pulse per revolution magnetic proximity sensor. A secondary relative position encoder was attached directly to the motor shaft. An ARL signal processing PLC module was used to convert the secondary encoder pulse output into analog position and velocity signals.

Freestream velocity was measured via total and static pressure measurements made variously using two absolute pressure transducers (prior to Test 21) or one differential pressure transducer (after Test 21 in order to reduce the uncertainty in the velocity measurement at low

Reynolds numbers). The total pressure signal came from a Kiel-type probe in the nozzle, and the static pressure signal from the far upstream static pressure taps in the test section.

All of the instruments were connected to an ARL data acquisition system which was used to record and pre-process the data. A description of the data acquisition system and its capabilities can be found in Appendix A. A detailed Sensor List relating measurements to channels, sensors, ranges, accuracies, and calibrations is included as Appendix B.

6.2 Numerical Model Description

Not applicable.

6.3 Test and Analysis Matrix and Schedule

The test matrix developed during ARL's sizing/scaling analysis of the hydrodynamics and drivetrain kinematics is shown in Table 1. The test matrix includes variations in 3 primary variables (reduced frequency, Reynolds number, and ratio of pitching/flapping magnitudes). Next, the effects of fin shape and orientation were explored by repeating the test condition matrix, with some variation as determined by the Test Engineer, for each of the fin configurations listed in Table 2. The number of conditions and combinations tested was limited in order keep within schedule/budget constraints (i.e. not N^4th test conditions).

Testing spanned approximately 1 month in the 12" water tunnel.

Table 1 – Matrix of test conditions

		Fin Mechanism Frequency (Hz)											
		Reduced Frequency assuming 2-inch Fin Chord											
		0.01	*0.02*	*0.03*	*0.05*	*0.08*	*0.13*	*0.22*	*0.36*	*0.60*	*1.00*		
U (m/s)	*1*	0.03	0.05	0.09	0.15	0.24	0.4	0.7	1.1	1.9	3.1	*60000*	**Chord Reynolds Number**
	2	0.06	0.10	0.17	0.29	0.5	0.8	1.3	2.3	3.8	6.3	*110000*	
	3	0.09	0.16	0.26	0.44	0.7	1.2	2.0	3.4	5.6	9.4	*170000*	
	4	0.13	0.21	0.35	0.6	1.0	1.6	2.7	4.5	7.5	13	*230000*	
	5	0.16	0.26	0.44	0.7	1.2	2.0	3.4	5.6	9.4	16	*280000*	
	6	0.19	0.31	0.52	0.9	1.5	2.4	4.0	6.8	11	19	*340000*	
	7	0.22	0.37	0.61	1.0	1.7	2.8	4.7	7.9	13	22	*400000*	
	8	0.25	0.42	0.70	1.2	1.9	3.2	5.4	9.0	15	25	*450000*	
	9	0.28	0.47	0.78	1.3	2.2	3.6	6.1	10	17	28	*510000*	
	10	0.31	0.52	0.87	1.5	2.4	4.0	6.7	11	19	31	*560000*	
		Red highlighted values exceed motor controllable speed range, or design flapping torque. Yellow values exceed mechanism design frequency.											

Table 2: Matrix of fin configurations

	Fin A	Fin B	Fin C	Fin D	Fin E
Pitch axis distance from leading edge (in)	0.31, <u>0.50</u>, 0.69	0.50	0.50	0.50	0.50

Pitch axis location (%mean chord)	17%, 27%, 38%	27%	25%	25%	25%
Sweep angle (deg)	-4, 0, 4	0	0	0	0
Pitch Ratio	2, 2.5	1.5, 2, 2.5, 3	2	2	2
*Parameters were varied singly from the underlined baseline configuration (where indicated)					

6.4 Safety

The water tunnel test conditions selected by experienced engineers and technicians to ensure they can be safely achieved with the facility and test setup. A finger-tight enclosure was constructed around the motor phase connections to minimize the danger of electrocution, and lock-out / tag-out procedures were followed before opening the enclosure. Mechanical hazards were minimized by disabling the motor drive before working on the pitching/flapping mechanism. Two test engineers were present at all times during tunnel operation. The test mechanism motor/generator controller was adjusted manually from a variable frequency drive mounted on the road side by the 48” water tunnel.

6.5 Contingency Plans

As with all experimental activities, especially with a new test setup, there is significant uncertainty and risk involved with budget and schedule. To mitigate these risks, a series of test readiness reviews between ARL and Pterofin were conducted via video teleconference prior to testing in order to prioritize test activities and ensure that critical parts of the testing were conducted early in order to minimize the impact of limited budget/schedule. As testing progressed, ARL and Pterofin continued to hold regular test update teleconferences to discuss progress and review preliminary data. One positive result of this collaboration was the selection and delivery by Pterofin of additional fin geometries to add chord length to the fin parameter space enabling the expansion of the test matrix to efficiently maximize results. Ultimately, all of the primary and secondary parameters were explored to some extent, except for flapping angle magnitude which was fixed due to budget constraints. We were also able to overcome unexpected events (such as a fin breaking off at the root) during testing.

6.6 Data Management, Processing, and Analysis

6.6.1 Data Management

Experimental data is stored on ARL’s secure network and serve as a backup repository. Data files are CSV format for DAQ data. The final deliverable data will be transferred via an external hard drive, optical disc, or upload to MHK-DR at the sponsor’s discretion.

6.6.2 Data Processing

Data collected was pre-processed in order to bring it into relevant engineering units with relevant corrections (i.e. windage and zero offset) and statistics (i.e. time averaging) for "Quick Look" reviews. The Test Engineer reviewed Quick Look data on a daily basis to identify and address any data acquisition or mechanical issues. Windage tests were conducted periodically as well as whenever significant hardware changes were made to the drivetrain in order to ensure we were capturing any drift in these corrections and monitoring the health of the system.

An in-situ calibration check was performed to verify the motor shaft torque measurement using as reference a calibrated torque wrench. The motor shaft speed was verified by differentiation of motor position.

The measurement uncertainty declared by the manufacturer of each instrument has been provided for reference in Appendix B.

6.6.3 Data Analysis

Pre-processed time-averaged run data were post-processed using Matlab. Post-processing of the time averaged run data consisted of the following steps:

Step 1: Calculate the windage offset Q_{wind} using the coefficients listed in Table 3

$$Q_{wind} = C_4 n_{rpm}^4 + C_3 n_{rpm}^3 + C_2 n_{rpm}^2 + C_4 n_{rpm} + C_1 \ (Nm)$$

where n_{rpm} = MotorEncRPM.

Table 3: Windage offset coefficients

Test No.	Pitch Pulley	C_4	C_3	C_2	C_1	C_0	Apply to Tests
1	28t	2.2703E-12	-7.0408E-09	7.9759E-06	-4.3735E-03	-8.6529E-01	4
6	23t	9.6731E-13	-3.4633E-09	4.5051E-06	-2.8778E-03	-1.2160E+00	8
9	28t	2.1839E-12	-7.1488E-09	7.8119E-06	-3.8968E-03	-9.9810E-01	10-18
20	23t	1.3947E-12	-4.5325E-09	4.8100E-06	-2.3151E-03	-5.9495E-01	22-24
27	18t	1.6696E-12	-5.4962E-09	5.8498E-06	-2.8427E-03	-5.9340E-01	25
29	38t	-1.2169E-13	-2.4978E-10	6.2385E-07	-8.5693E-04	-9.2603E-01	30

33	28t	2.2361E-12	-5.8101E-09	5.2869E-06	-2.9465E-03	-1.0790E+00	34-36,41

Step 2: Recalculate the motor torque from the motor torque signal (because it was calculated incorrectly before Pterofin018) and subtract the windage torque for each run

$$Q_{motor} = 10.027798 \; x \; Torque_{Signal} - Q_{wind} \; (Nm)$$

Step 3: Calculate system performance metrics

Motor power where a positive value represents power extracted (turbine) and a negative value represents power expended (pump)

$$P_{motor} = \frac{0.7376 \, Q_{motor} \, n_{rpm}}{5252} \; (hp)$$

The power coefficient having the same sign convention

$$Cp = \frac{550 \, P_{motor}}{\frac{1}{2}\rho Vinf^3 A_{swept}} \; (dimensionless)$$

where $A_{swept} = 0.256 \, ft^2$.

The torque coefficient is

$$K_Q = \frac{0.7376 \, Q_{motor}}{\rho(\frac{n_{rpm}}{60})^3 D_{tip}^5} \; (dimensionless)$$

where $D_{tip} = 1.98 \, ft$. The Reynolds number based on fin chord length and freestream velocity is

$$Re_c = \frac{c_{fin} \, V_{inf}}{\mu} \; (dimensionless)$$

Finally we calculated the fin reduced frequency based on fin chord length, fin angular velocity (one half of motor angular velocity), and free stream velocity

$$k = \frac{c_{fin} \, n_{rpm} \, \pi}{60 \, V_{inf}} \; (dimensionless)$$

Figures showing the time averaged motor torque, RPM, power coefficient, and torque coefficient as functions of reduced frequency for all tests can be found in Appendix C.

Pre-processed time series data from each run were post-processed using Matlab scripts. Post-processing of the time series run data to generate phase-averaged figures consisted of the following steps:

1. Fit a Fourier series having eight terms to *MotorHomeEnc* and then locate the pulse peaks. Since the motor frequency doubles that of the fin every other peak represents the start of a fin oscillation cycle.

2. Calculate the motor torque and system performance metrics for each time step as previously described above for the time averaged analyses.

3. Interpolate the motor torque and system performance metrics to integer *Position* motor angles using a shape-preserving piecewise cubic spline.

4. Phase-average the motor torque and system performance metrics for fin oscillation periods beginning with every other MotorHomeEnc pulse peak.

7 Project Outcomes

7.1 Results

The projects' overall objective was to build up a dataset of hydrodynamic performance across a range of primary design variables:

- Reduced frequency
- Ratio of flapping/pitching angle magnitude
- Reynolds number

Figure 10 shows how the power coefficient is defined in order to be consistent with conventions from other common devices used to extract kinetic energy from fluid flows. In this case, the swept area of the flapping hydrofoil is used in the denominator to be consistent with conventions for wind and hydrokinetic turbines in order to size the amount of flow passing through the machine available to extract power. The freestream incoming velocity is used in the denominator. The mechanical shaft power delivered at the blade/foil is in the numerator.

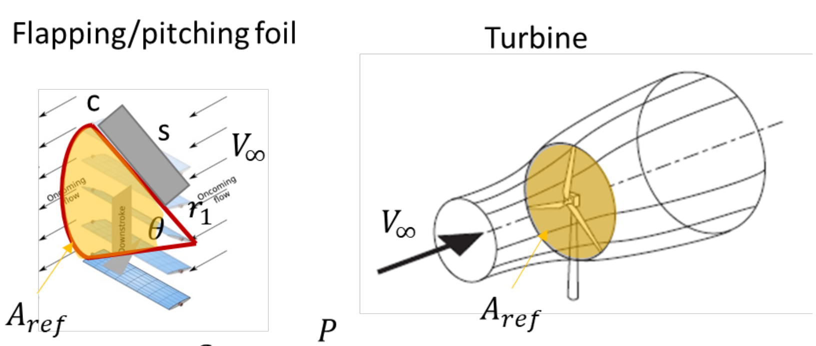

$$C_P = \frac{P}{\frac{1}{2}\rho V_\infty^3 A_{ref}}$$

Figure 10: Power Coefficient Definition

Figure 11 shows a representative example of non-dimensional performance (power coefficient) results from the flapping/pitching hydrofoil (figures on right) compared with a typical performance plot for wind turbine (figure on left). The reduced frequency and the tip speed ratio are the non-dimensional metric that sets the kinematics (i.e. the local instantaneous flow relative to the foil orientation which determines the lift and drag). Power coefficient increases with reduced frequency until it reaches a local maximum value and begins to decrease. Power coefficient eventually becomes negative at higher reduced frequency as the flapping/pitching hydrofoil begins to put energy into the flow and produce thrust. The point where this transition occurs is essentially when the net lift coefficient on the foil switches sign. When Reynolds number is sufficiently high (in the hundreds of thousands), the performance curves collapse and non-dimensional performance is insensitive to Reynolds number. Some of the earlier tests show greater Reynolds sensitivity at low tunnel velocities, but this may be due primarily to high uncertainty in velocity measurements based on differential pressure. The dynamic pressure at low velocities were small relative to the pressure transducer resolution in early test cases until a lower range differential pressure transducer was substituted.

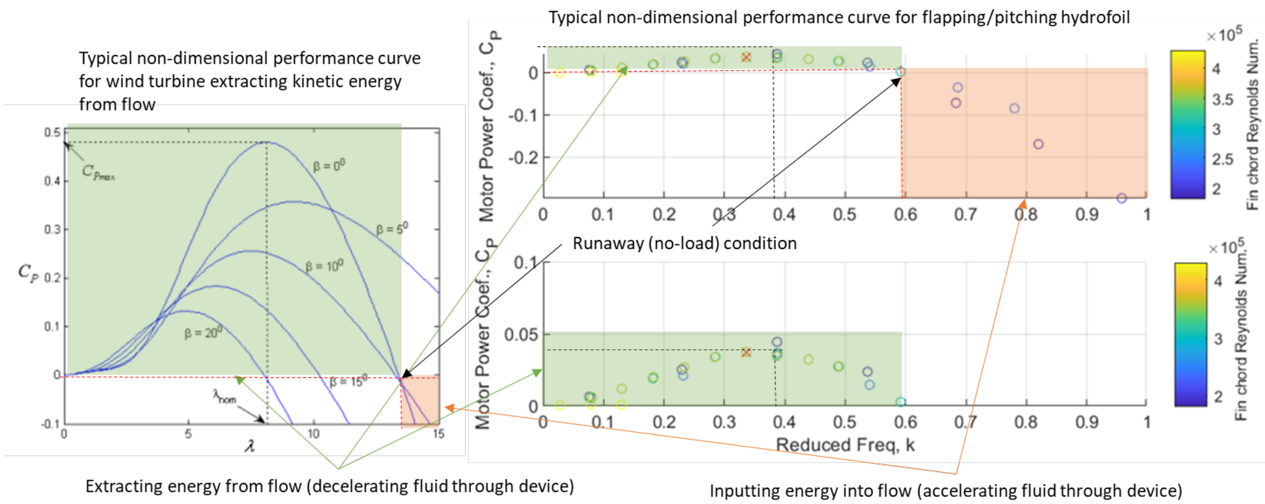

Figure 11: Typical non-dimensional performance curves for comparison of regions of operation

Figure 12 shows the local maximum pressure coefficient values and corresponding reduced frequency from the non-dimensional performance sweeps of a range of test configurations. This summary shows a clear trend where maximum power coefficient increases as reduced frequency increases. These peak conditions occur at reduced frequencies substantially above the typical range for quasi-steady flow approximation ($k < 0.05$). This implies that unsteady fluid flow physics are having a significant impact on performance, although decoupling the unsteady effects of the foil boundary layer development from the unsteady motion kinematics is only seen by looking at the tests using flat plate fins of differing chord (foils C, D, E). The scatter shown is the result of the various secondary design variables altered including:

- Chord or aspect ratio of hydrofoil
- Shape of the hydrofoil planform
- Hydrofoil position relative to pitching axis
- Hydrofoil sweep angle relative to pitching axis

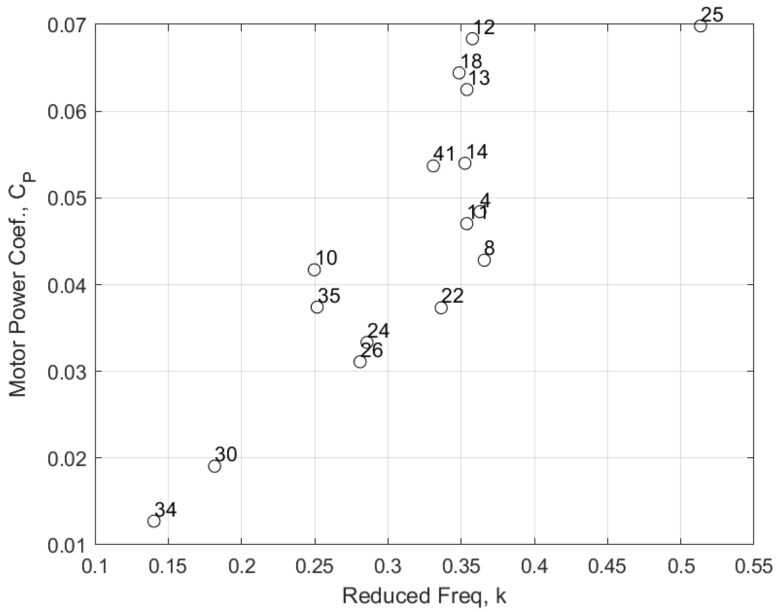

Figure 12: Summary of peak power coefficient values (ReC > 200,000) for all configurations tested as a function of reduced frequency and annotated with test number.

Figure 13 shows the maximum power coefficient as a function of the ratio between the pitching and flapping amplitudes. There does appear to be significant scatter in this data, although test 18 may be an outlier due to significant uncertainty in the velocity measurement with this test. The velocity measurement was calculated using Bernoulli's equation from a differential pressure. The differential pressure was very small relative to the transducer range, leading to a potentially low signal/noise ratio.

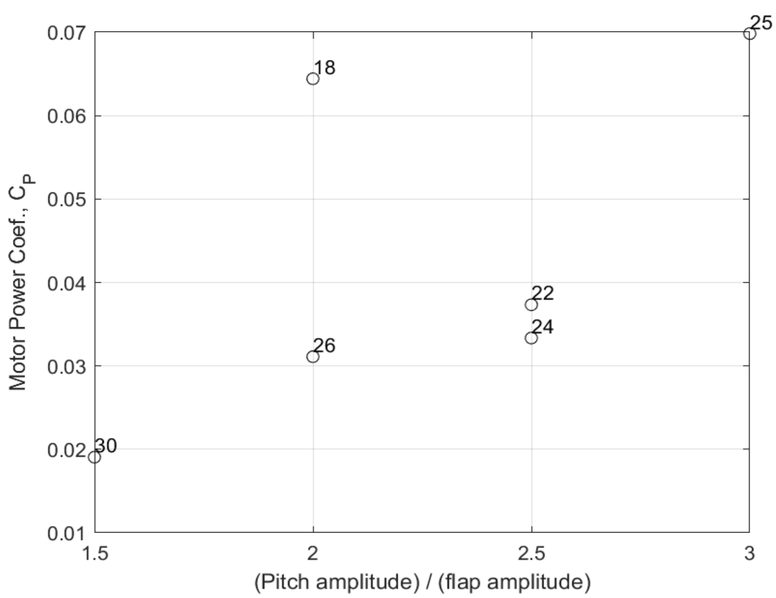

Figure 13: Peak power coefficient (ReC > 200,000) of Fin B as a function of relative pitch amplitude and annotated with test numbers. Note that test 18 used a different velocity measurement technique than the remainder.

Figure 14 shows the maximum power coefficient as a function of varying the chord of the hydrofoil while keeping the span and drivetrain motion constant. Changing the chord of the foil while keeping the span, fluid velocity, and flapping/pitching frequency constant allowed one to vary the reduced frequency while maintaining the same foil kinematics relative to the fluid.

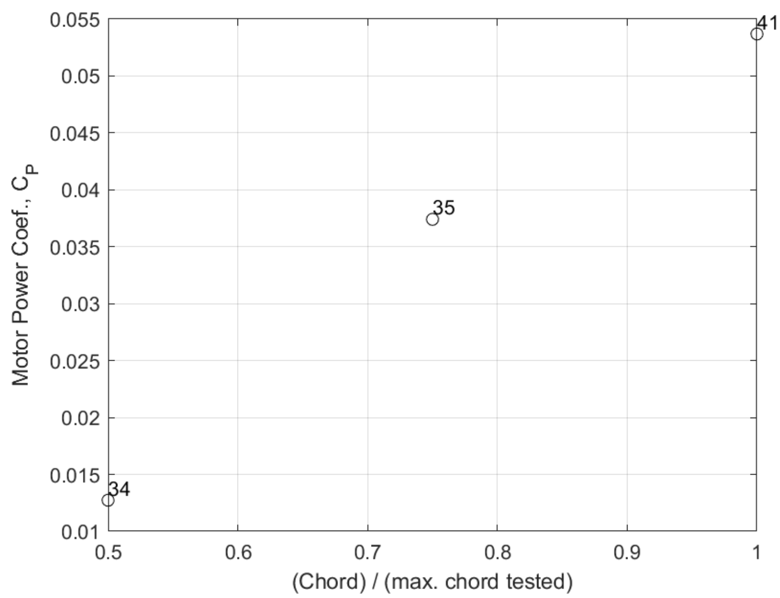

Figure 14: Peak power coefficient (ReC > 200,000) of flat plates as a function of relative chord length and annotated with test numbers.

In all, 7 independent parameters (primary plus secondary design variables) selected by Pterofin were varied to explore the design space experimentally. This 7 dimensional design space was sparsely interrogated based within limits of the test assembly and ultimately constrained by budget and schedule. It should be noted that additional design parameters were identified as potentially worthy of investigation, but unable to be tested due to practical constraints. Specifically, the flapping amplitude and the pitch scheduling relative to the flapping motion were not varied during testing.

7.2 Lesson Learned and Test Plan Deviation

- We underestimated the cost of the pitching/flapping mechanism design and fabrication due to the complexity of the motion requirements, and also to inflation in fabrication costs. Effort was shifted from modeling and reporting tasks to cover the excess. In addition, flapping arc length was also eliminated as a primary variable in the test matrix to reduce fabrication cost. Budgeting the cost of building something that has not yet been designed is always a challenge, but in the future we can use the actual cost data to scale estimates based on the number of simultaneously controlled motion axes.

- It was not possible to reliably calculate the exact position of the fin based on mechanism kinematics because the phase of the fin motion relative to the motor shaft could not be determined without additional sensors. If possible, additional position measurements should be made closer to or optimally on the fin itself. Without knowledge of the absolute fin position the post-processed phase averaged data were referenced to the motor shaft position instead.
- Aluminum was selected for its high strength to weight ratio as the material for the construction of fins / hydrofoils. In this application the high frequency, unsteadiness, and reversing nature of the load resulted in the loss of a fin due to fatigue. Future tests of a similar nature could utilize a material with a defined fatigue limit, or a significant factor of safety for the anticipated load and number of cycles. This experience highlighted a potential design consideration for any Pterofin device, where the phase locked maximum load may be far higher than the time average load. A large amplitude unsteady cyclic stress may drive the mechanical design of the hydrofoil.

8 Conclusions and Recommendations

Test data showed that maximum power coefficient occurred at reduced frequencies between about 0.2 and 0.5 and had peak power coefficient values between 0.02 and 0.07. The peak power coefficient occurred at reduced frequencies associated with highly unsteady flows, but continuing to increase the reduced frequency past the peak value led to a decrease in power coefficient (with the values eventually turning negative as the device sends power into the fluid). Increasing the reduced frequency at which the maximum power coefficient occurred increased the peak value. It should be noted that the reduced frequency effectively sets the kinematics of the blade relative to the fluid in this configuration.

It should be noted that the absolute magnitude of the power coefficient of the compound pitching/flapping hydrofoil was substantially lower than traditional turbines designed to extract kinetic energy from fluid flows. This is not necessarily unexpected because the specific pitching/flapping hydrofoil designed and tested was intended to be canonical and not optimized for maximum efficiency (in part because of the lack of sufficient design relevant data motivating the test). It does highlight the fact that the ratio of lift to drag is more closely related to the efficiency of power extraction than the maximum lift coefficient.

In other words, hydrofoils designed to take advantage of unsteady boundary layer development may allow one to operate at very high lift coefficients, but this does not necessarily lead to increased hydrodynamic efficiency. Physically, this means that it may be easier to design a wing/foil/blade to operate at a maximum lift/drag ratio in a turbine configuration where the relative velocities and blade section angles of attack are known and steady in the blade relative reference frame. In a pitching/flapping foil, these angles are always changing in time and along the span. In a pitching/flapping hydrofoil, this could be accomplished by actively twisting the foil during its motion and/or having increase fidelity and control over the pitch motion scheduling relative to the flapping motion.

The reduced frequency range that the maximum power coefficient occurs at is relatively insensitive to all the design parameters that were varied (ratio of pitching/flapping, foil shape, foil orientation). This implies that the cross section and planform of the foil are not critical design parameters. This does indicate that the hydrodynamic shaping of the foil cross section is not critical and significant cost savings could be gained with simple plate-like foil shapes. The aspect ratio of the foil and/or the flapping amplitude are more likely candidates for being primary design parameters that influence the power coefficient. Reynolds number effects were not readily apparent above the turbulent transition range of approximately 200k (effectively insensitive), although the signal-to-noise ratio of the data at low Reynolds numbers make it difficult to interpret these parts of the datasets.

Test data showed that the phase locked average torque amplitude was much higher than the time average torque. This implies that the designer needs to seriously consider the unsteady forces and moments when designing the mechanical structures of the system, rather than simply the time average loads. As an example, one foil broke off at the root during testing even though we were well away from the mechanical limit. This was likely due to fatigue loading of the aluminum, which has no endurance limit, combined with potential stress concentrations due to the attachment features.

Investigation of the phase locked average torque signal indicates that most of the power extracted may occur in specific parts of the compound motion (i.e. a power stroke) with other regions contributing minimal amounts of power or even sending power in the opposite direction (actively working against the device). This implies that increasing the absolute level of the power coefficient may require defining a specific scheduling of the pitching relative to the flapping motion. The knowledge of how to do this with a simple drivetrain/mechanism could be valuable proprietary technologies for Pterofin to develop.

9 References

• References

[1] J. R. Brodell and A. H. Soni, "Design of the crank-rocker mechanism with unit time ratio," *Journal of Mechanisms,* vol. 5, no. 1, pp. 1-4, 1970.

10 Acknowledgements

The authors would like to thank David DeVilbiss, Brian Kline, and Amber Miller for their assistance in the areas of instrumentation and data acquisition. The accomplishments listed herein would not have been possible without the efforts of the Garfield Thomas Water Tunnel Facility Support Group including Matthew Brumbaugh, Curtis Connacher, James Mickey, and Michael Prendergast.

11 Appendix

Appendix A – Data Acquisition System Description

Test data were acquired using a National Instruments CompactDAQ chassis containing multiple modules for acquiring different types of signals. Analog signals were measured using an NI9205 Analog I/O Module comprising 16 differential or 32 single ended 16 bit analog to digital channels. Each channel can sample a range of voltages from -10V to +10V with an accuracy of +/- 6230μV at a rate of up to 250 kS/s. Digital Channel 14 ("Position") pulses were counted using an NI9411 Digital I/O Module comprising 6 differential or single-ended input channels, each supporting a maximum update rate of 500 ns. Heise DXD absolute pressure transducers were polled via an RS-232 serial interface, and are also listed under "digital channels" in Appendix B.

Data were recorded at a rate of 2 kHz using a custom interface (WTDAQ) programmed in National Instruments LabVIEW and MATLAB, and running on a Windows PC. WTDAQ enables the operator to record, label, pre-process, and view data in real-time. WTDAQ generates a folder structure for every test the follows the pattern:

Folder structure: //YYYY/MM/DD/Pterofin**TTTT**/
(**Y** = Year, **M** = Month Number, **D** = Day Number, **T** = Test Number)

Within the test folder files are generated specific to the test configuration and measurements:

Pterofin_**DDMMMYYYY**.xls, test configuration, including a channel list and pre-processing equations to convert voltage measurements to engineering units.
(**Y** = Year, **M** = Month Text, **D** = Day Number)

Pterofin**TTT**_LOG.csv, operator's log. When there is disagreement between an individual test log and the overarching test log the overarching test log has precedence.

Pterofin**TTT**_MEAN.csv, time averaged values, one row for each run.

Pterofin**TTT**_STD.csv, standard deviation from mean values, one row for each run.

Pterofin**TTT**R**rrr**.csv, time series of data, one file for each run.
(**T** = Test Number, **r** = Run Number)

Pterofin**TTT**R**rrr**_zero.csv, time series of data for zeroes, one or more files per test.
(**T** = Test Number, **r** = Run Number)

In a typical test the operator acquires a “zero” run in the quiescent state. The mean values of analog channels 2 (“Torque_Signal”) and 7 (“DifferentialP”) if present are subtracted from all subsequent recordings of those channels as an offset. If another “zero” run is acquired then the newly acquired offset will apply to all of the following (but none of the preceding) runs.

The test number increments every time the DAQ operator records data. Tests during which the operator was simply performing routine system checks or troubleshooting problems have not be included in this report.

Note: The DAQ test configuration file changed several times during the test for various reasons. The MEAN, STD, and time series data files listed above have been pre-processed according to the relevant test configuration, a list of changes to the configuration files and pre-processed data can be found in Table 4. When possible the post-processed data is consistent with the latest test configuration.

Table 4: Cumulative changes to test configuration files.

Test Configuration file name (.xls)	Tests	Change Description	Reason for change	Pre-processed values impacted
PteroFin_20Jun2023	1-14	Baseline configuration.		
PteroFin_30Jun2023	18-20	Removed excitation scaling from the formula for “Torque_Nm”	Amplified sensor was incorrectly scaled by excitation.	Torque_Nm, Torque_FtLbf
PteroFin_5Jul2023	22-42	Added sensor “DifferentialP” and substituted “DifferentialP” for “PSAvg” in the formula for “Vinf”.	To reduce uncertainty and noise in the freestream velocity measurement.	DifferentialP (new), Vinf

The data acquisition needs of this project were to measure and record multiple analog, digital, and TTL channels on a common time base at a frequency of 2 kHz. WTDAQ connected to the NI devices described above meets or exceeds these needs.

Table 5 and Table 6 list of all the sensors recorded by analog and digital channels respectively, sensor type, range, accuracy, and calibration date and method if applicable. Table 7 lists the formulas used to pre-process the data.

Table 5: Analog channel list

Analog Channel	Name	Symbol	Units	Type	Measurement	Sensor Make/Model	S/N	Location	Range +/- Accuracy	Cal. Date, Method
1	Water Temperature		°F	RTD	Water temperature	StoLab PL		Nozzle centerline	-85 to 200 +/- 0.10C	
2	Torque_Signal		V	Strain gage	Motor shaft torque	Futek TRS605-FSH-02057	1039239	Motor output shaft	-50 to 50 Nm +/- 0.3% F.S.	3/30/2023, dead weight.
3	HomePulse		V	Magnetic proximity	Motor shaft index pulse	Contrinex DW-AD-502-M5		Motor output shaft		
4	EncBoxRPM	n_{rpm}	RPM	Processed relative encoder output	Motor shaft speed			Motor input shaft		
5	EncBox Position		degrees	Processed relative encoder output	Motor shaft rel. pos.			Motor input shaft		
6	Torque_Excite		V	Analog voltage	Torque excitation voltage	N/A		Motor output shaft		

Testing & Expertise for Marine Energy

7	DifferentialP		psid	Strain gage	(Kiel Ptotal) - (Test section Pstatic)	Sensotec FDW1AV,2D5D6Q	995617	Nozzle and test section	-10 to 10 PSIA +/- 0.1%	Nominal 2psi/V sensitivity.

Table 6: Digital channel list

Digital Channel	Name	Units	Type	Measurement	Sensor Make/Model	S/N	Location	Range +/- Accuracy	Cal. Date, Method
1	PT	psia	Absolute pressure	Keil total pressure	Heise DXD	40	Nozzle	0-100 psia +/- 0.02% F.S.	3/27/2019, Ruska reference source.
2	PSU1	psia	Absolute pressure	Test section wall static pressure	Heise DXD	41	Upper console port 1	0-100 psia +/- 0.02% F.S.	8/22/2018, Ruska reference source.
3	PSU2	psia	Absolute pressure	Test section wall static pressure	Heise DXD	42	Upper console port 2	0-100 psia +/- 0.02% F.S.	8/22/2018, Ruska reference source.
4	PSU3	psia	Absolute pressure	Test section wall static pressure	Heise DXD	43	Upper console port 3	0-100 psia +/- 0.02% F.S.	3/27/2019, Ruska reference source.
5	PSU4	psia	Absolute pressure	Test section wall static pressure	Heise DXD	44	Upper console port 4	0-100 psia +/- 0.02% F.S.	1/29/2019, Ruska reference source.
6	PSU5	psia	Absolute pressure	Test section wall static pressure	Heise DXD	45	Upper console port 5	0-100 psia +/- 0.02% F.S.	4/8/2019, Ruska reference source.

7	PSU6	psia	Absolute pressure	Test section wall static pressure	Heise DXD	46	Upper console port 6	0-100 psia +/- 0.02% F.S.	4/8/2019, Ruska reference source.
8	PSL1	psia	Absolute pressure	Test section wall static pressure	Heise DXD	47	Lower console port 1	0-100 psia +/- 0.02% F.S.	6/25/2019, Ruska reference source.
9	PSL2	psia	Absolute pressure	Test section wall static pressure	Heise DXD	49	Lower console port 2	0-100 psia +/- 0.02% F.S.	4/28/2021, Ruska reference source.
10	PSL3	psia	Absolute pressure	Test section wall static pressure	Heise DXD	35	Lower console port 3	0-100 psia +/- 0.02% F.S.	1/29/2019, Ruska reference source.
11	PSL4	psia	Absolute pressure	Test section wall static pressure	Heise DXD	36	Lower console port 4	0-100 psia +/- 0.02% F.S.	4/28/2021, Ruska reference source.
12	PSL5	psia	Absolute pressure	Test section wall static pressure	Heise DXD	37	Lower console port 5	0-100 psia +/- 0.02% F.S.	3/26/2021, Ruska reference source.
13	PSL6	psia	Absolute pressure	Test section wall static pressure	Heise DXD	38	Lower console port 6	0-100 psia +/- 0.02% F.S.	8/22/2018, Ruska reference source.

14	Position	degrees	Angle	Motor shaft relative position	Futek TRS605-FSH-02057	1039239	Motor output shaft		

Table 7: Pre-processing formulas

Formula Number	Result Name	Symbol	Units	Formula String
1	Density	ρ	slugs/ft^2	lookup table
2	Viscosity	v	ft^2/sec	lookup table
3	VaporPressure		psia	lookup table
4	PSavg		psia	(PSU1+PSL1)/2
5	Vinf	V_{inf}	ft/s	12*sqrt(abs(DifferentialP)/(0.5*ρ))
6	Position		degrees	(hardcoded in WTDAQ)
7	Torque_Nm		Nm	Torque_Signal*10.027798
8	Torque_FtLbf		ft-lbf	Torque_Nm*0.7376

Appendix C – PROCESSED DATA: TIME AVERAGED VALUES

The following figures show the time averaged values resulting from analysis of pre-processed test data. Each figure corresponds to a single test, which typically corresponds to a single fin and mechanism configuration. Each test constitutes multiple runs with each run corresponding to a single mechanism and tunnel condition (Reynolds number and reduced frequency). Reynolds number based on maximum blade chord length was varied during each test by changing free stream velocity. At each Reynolds number the reduced frequency was varied by changing motor RPM. The point corresponding to the run of maximum power coefficient (with Reynolds number > 200,000) is indicated in each subplot with a red "x".

For further processing or plotting tables of time averaged pre-processed test data (motor torque, motor RPM, freestream velocity, system performance metrics (tared motor torque, Reynolds number, reduced frequency, power coefficient, and torque coefficient) can be found in comma separated variable files for each test in a folder structure corresponding to the date the test was conducted. For example, for test "Pterofin004" the pre-processed data can be found in the deliverable data file system, subfolder:

/2023/06/22/Pterofin0004/Pterofin004_MEAN.csv

The system performance metrics derived from the pre-processed test data are located in the same folder, filename:

Pterofin004_MEAN_TARED.csv

Due to uncertainty in the pressure based measurement of freestream velocity only cases with Vinf > 3 ft/s are included in the following figures.

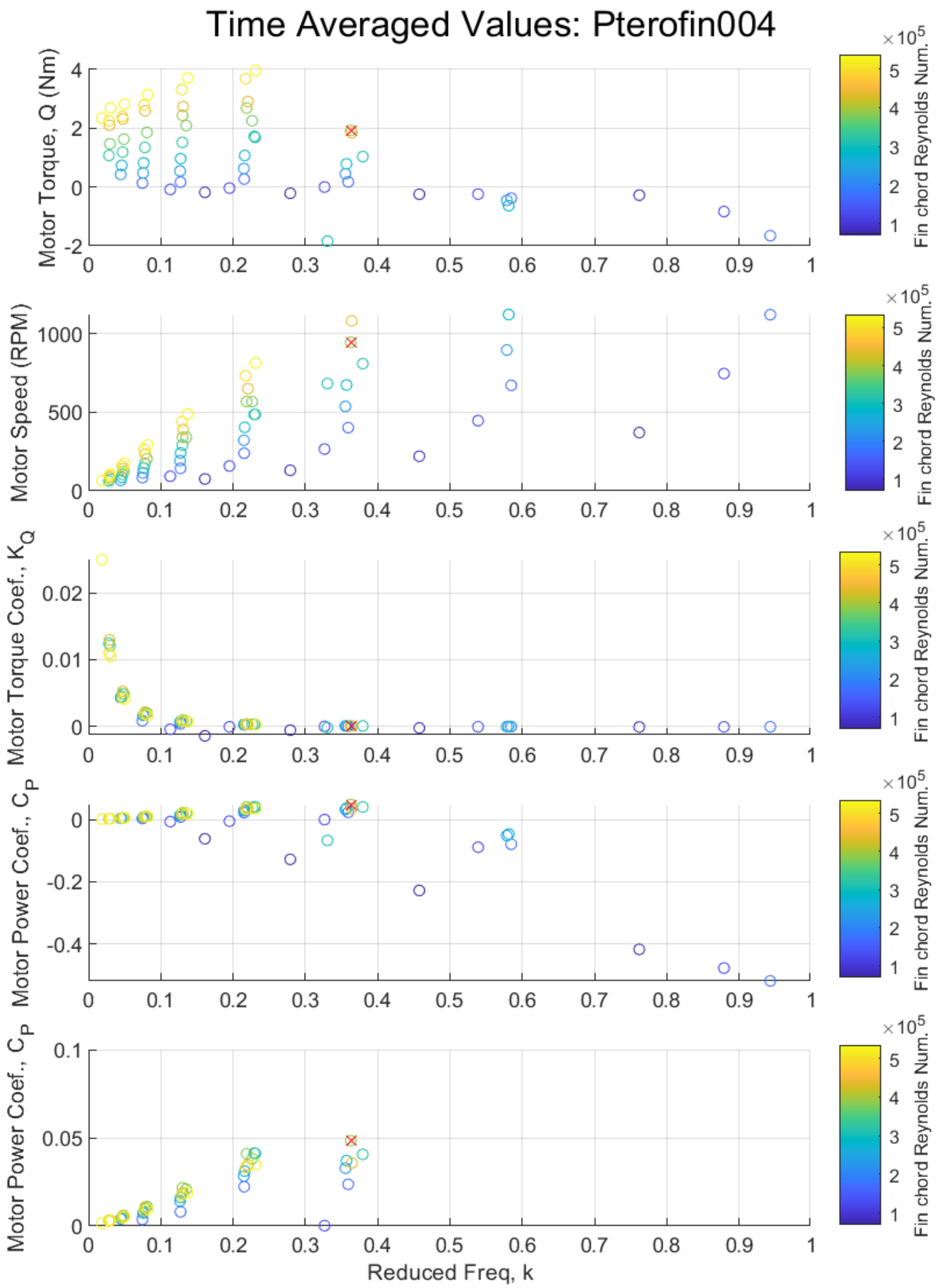

Time Averaged Values: Pterofin004
Motor Torque, Q (Nm)
Motor Speed (RPM)
Motor Torque Coef., K_Q
Motor Power Coef., C_P
Motor Power Coef., C_P
Reduced Freq, k
Fin chord Reynolds Num.
$\times 10^5$

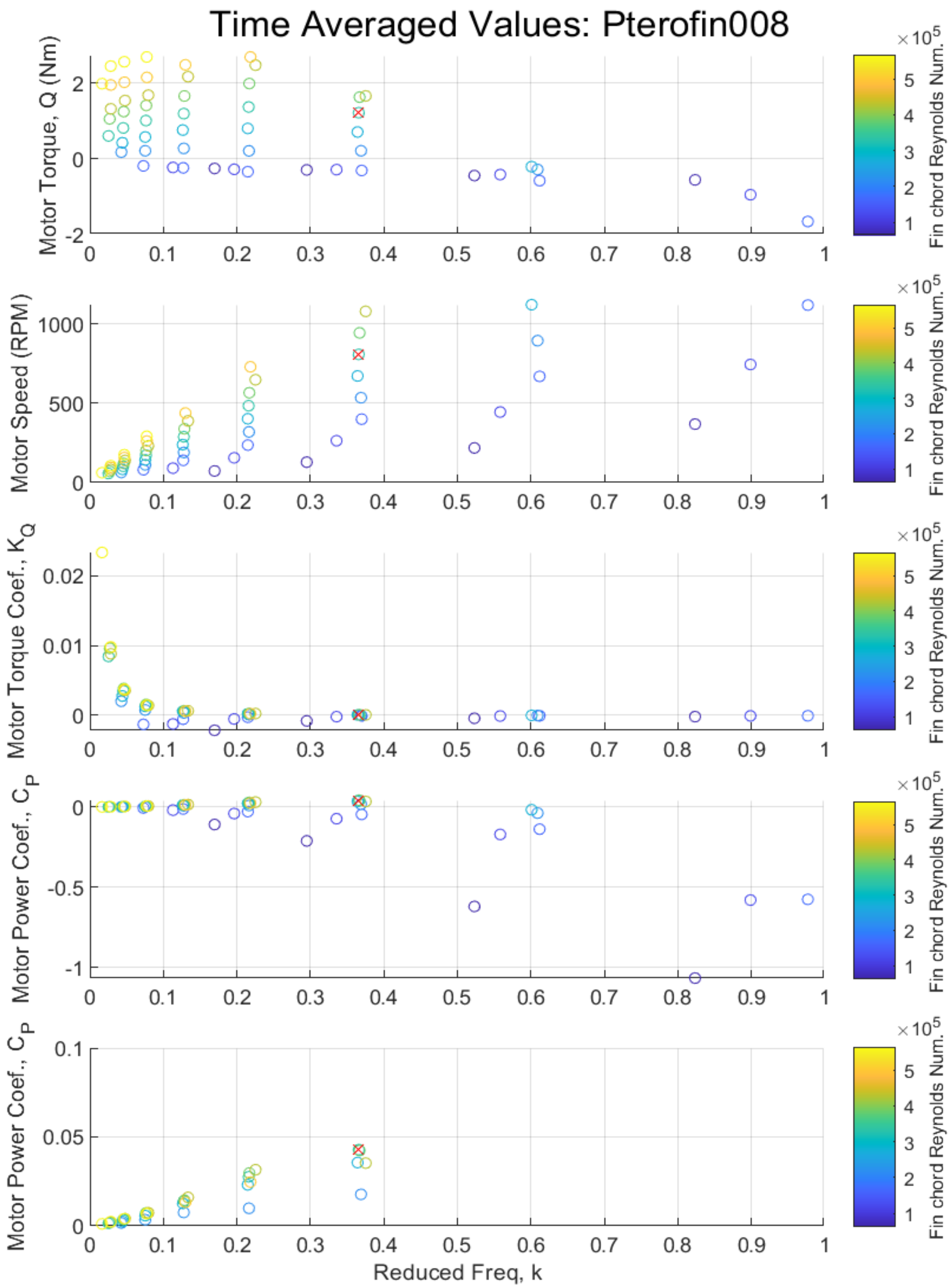
Time Averaged Values: Pterofin008
Motor Torque, Q (Nm)
Motor Speed (RPM)
Motor Torque Coef., K_Q
Motor Power Coef., C_P
Motor Power Coef., C_P
Reduced Freq, k
Fin chord Reynolds Num.
×10^5

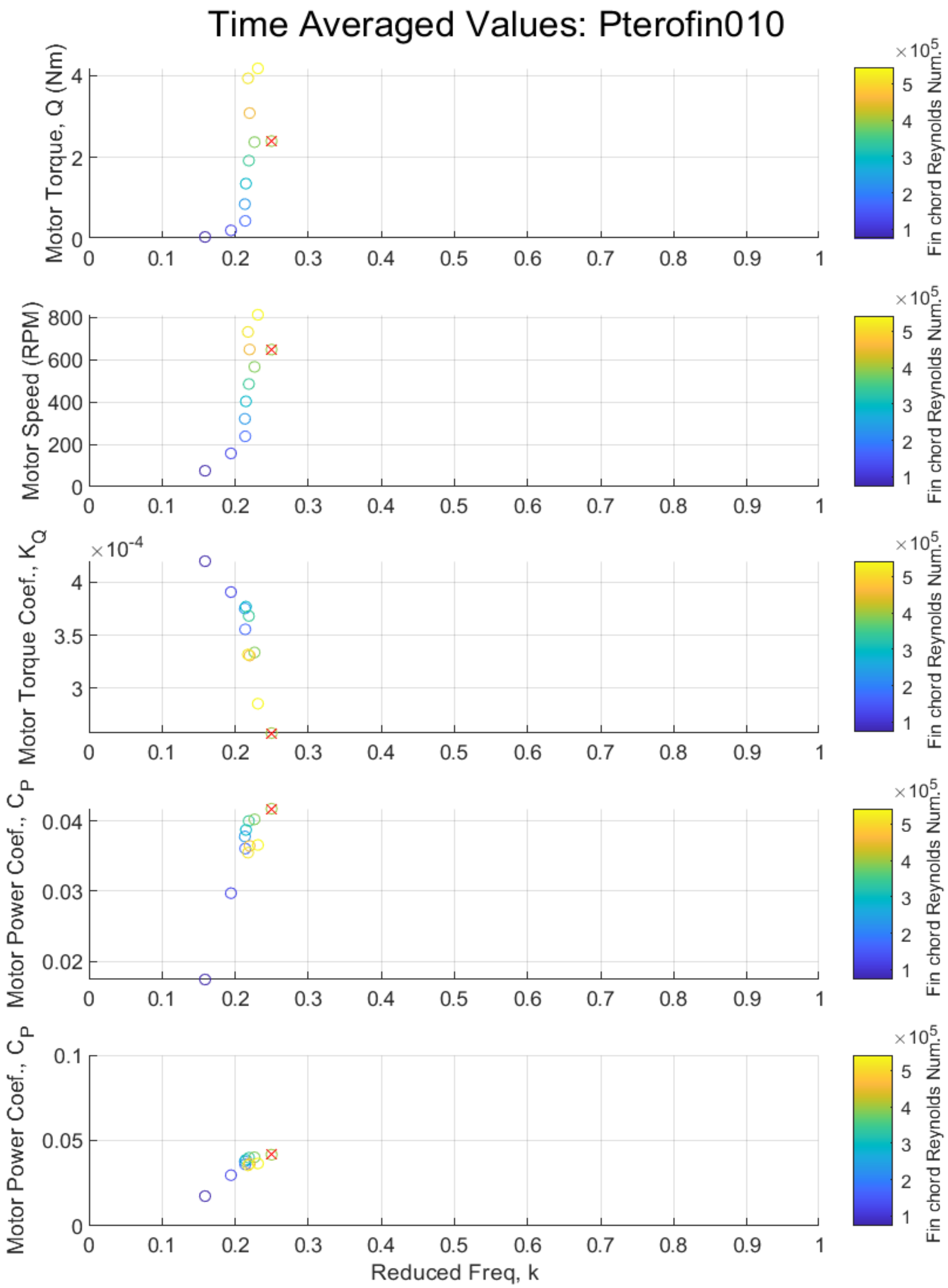
Time Averaged Values: Pterofin010
Motor Torque, Q (Nm)
Motor Speed (RPM)
Motor Torque Coef., K_Q
Motor Power Coef., C_P
Motor Power Coef., C_P
Reduced Freq, k
Fin chord Reynolds Num.
$\times 10^5$
$\times 10^{-4}$

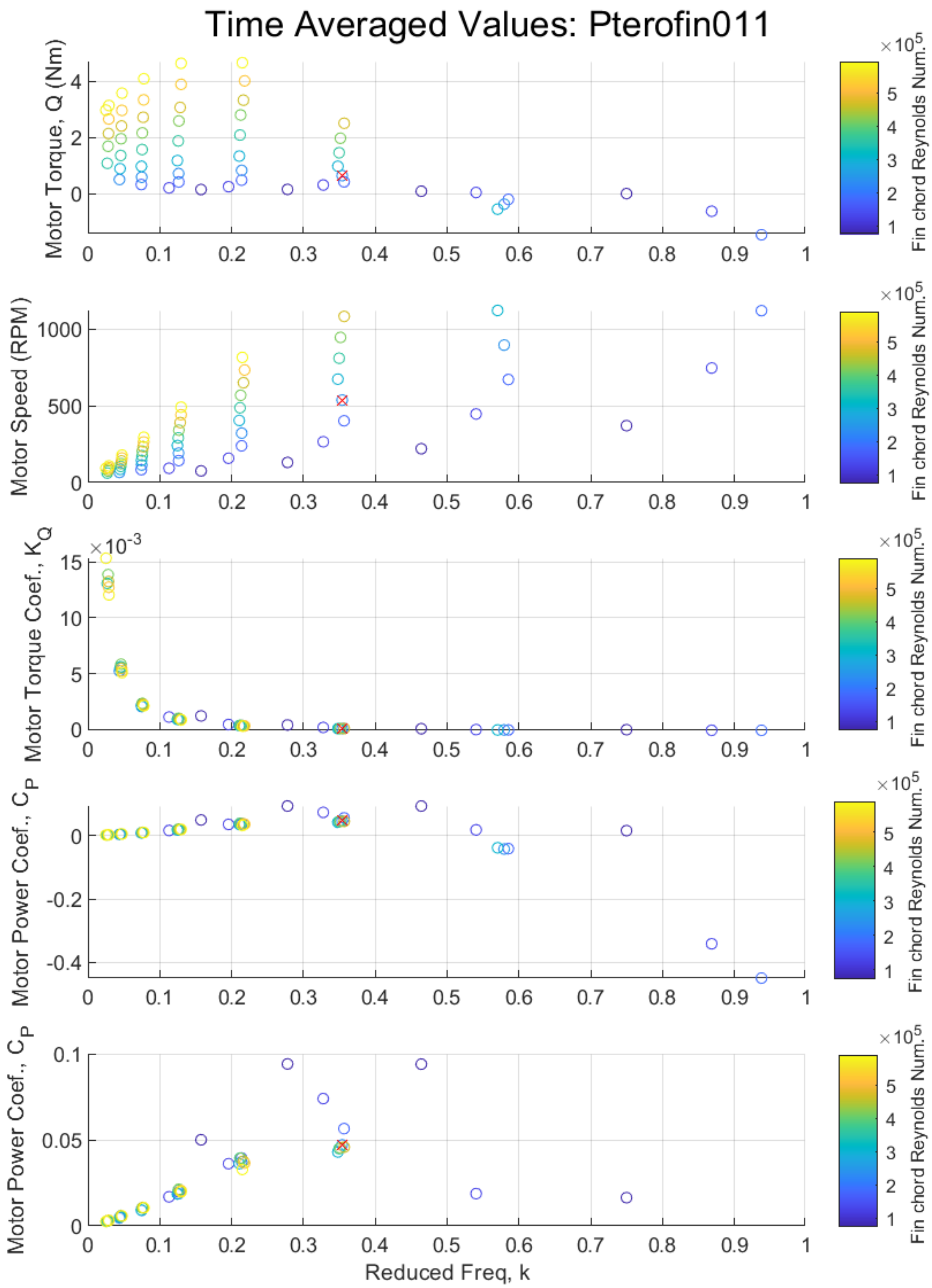
Time Averaged Values: Pterofin011
Motor Torque, Q (Nm)
Motor Speed (RPM)
Motor Torque Coef., K_Q
$\times 10^{-3}$
Motor Power Coef., C_P
Motor Power Coef., C_P
Reduced Freq, k
Fin chord Reynolds Num.
$\times 10^5$

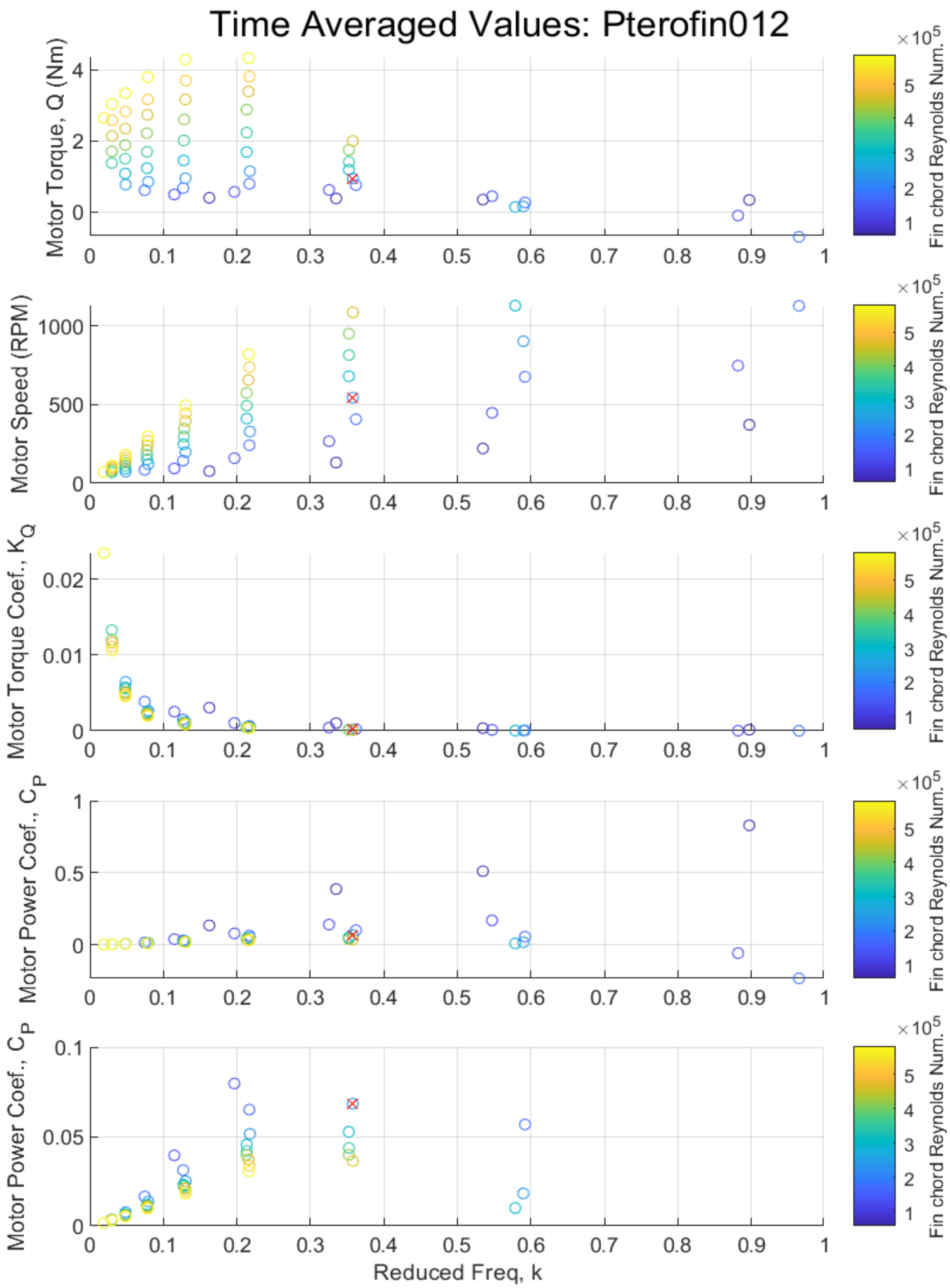

Time Averaged Values: Pterofin012
Motor Torque, Q (Nm)
Motor Speed (RPM)
Motor Torque Coef., K_Q
Motor Power Coef., C_P
Motor Power Coef., C_P
Reduced Freq, k
Fin chord Reynolds Num.
$\times 10^5$

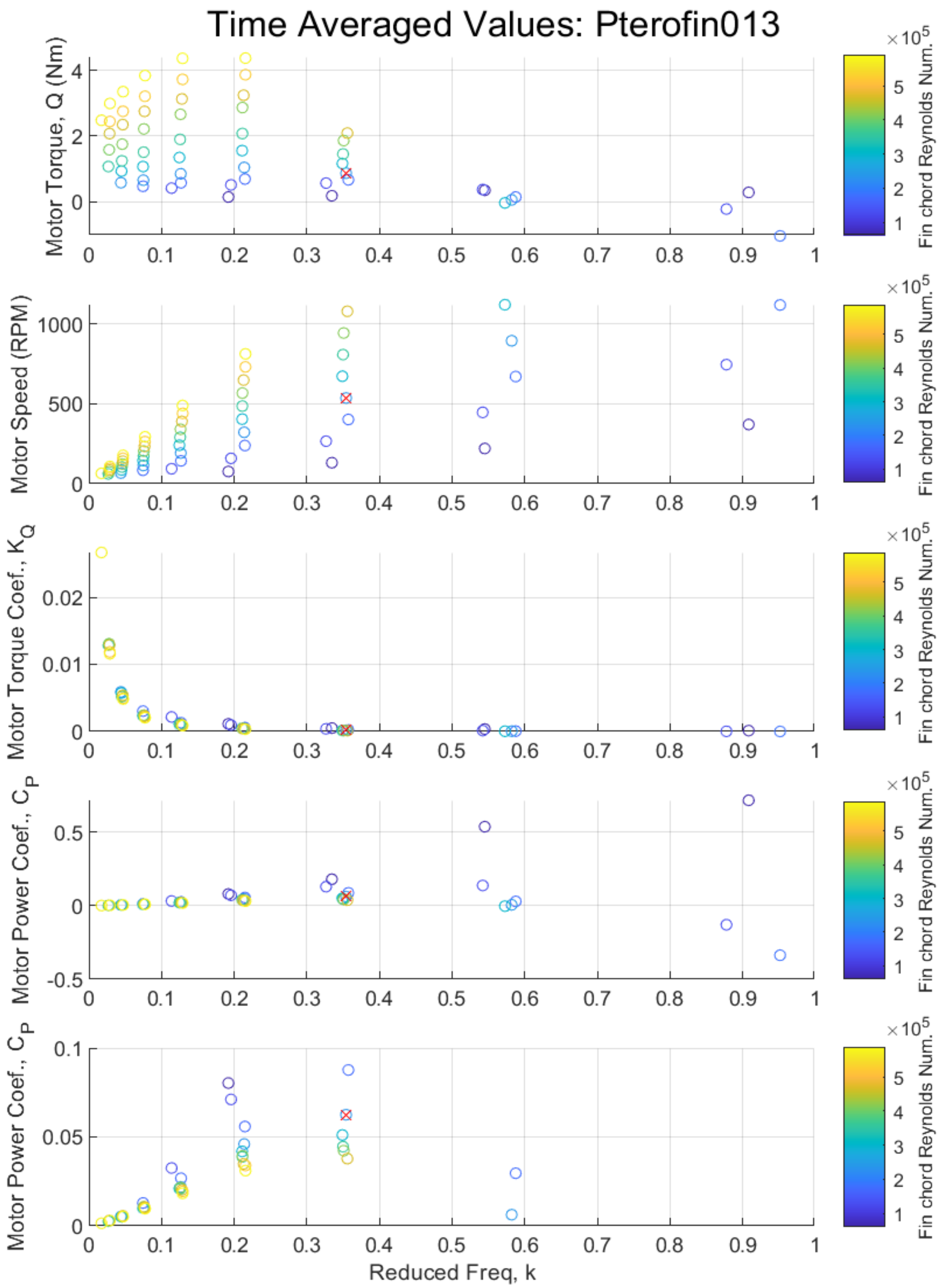

Time Averaged Values: Pterofin013
Motor Torque, Q (Nm)
Motor Speed (RPM)
Motor Torque Coef., K_Q
Motor Power Coef., C_P
Motor Power Coef., C_P
Reduced Freq, k
Fin chord Reynolds Num.
$\times 10^5$

TEAMER
Testing & Expertise for Marine Energy

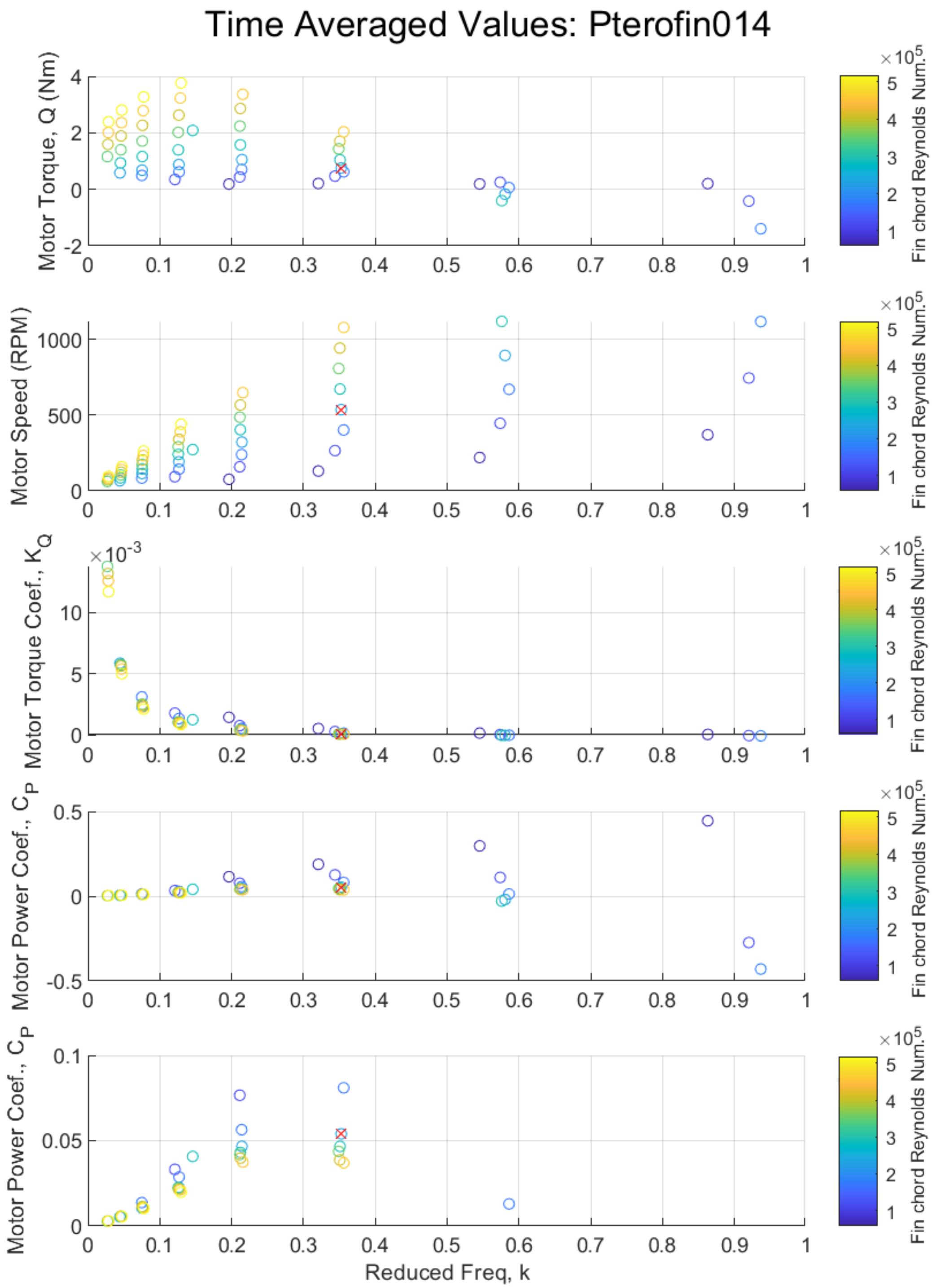

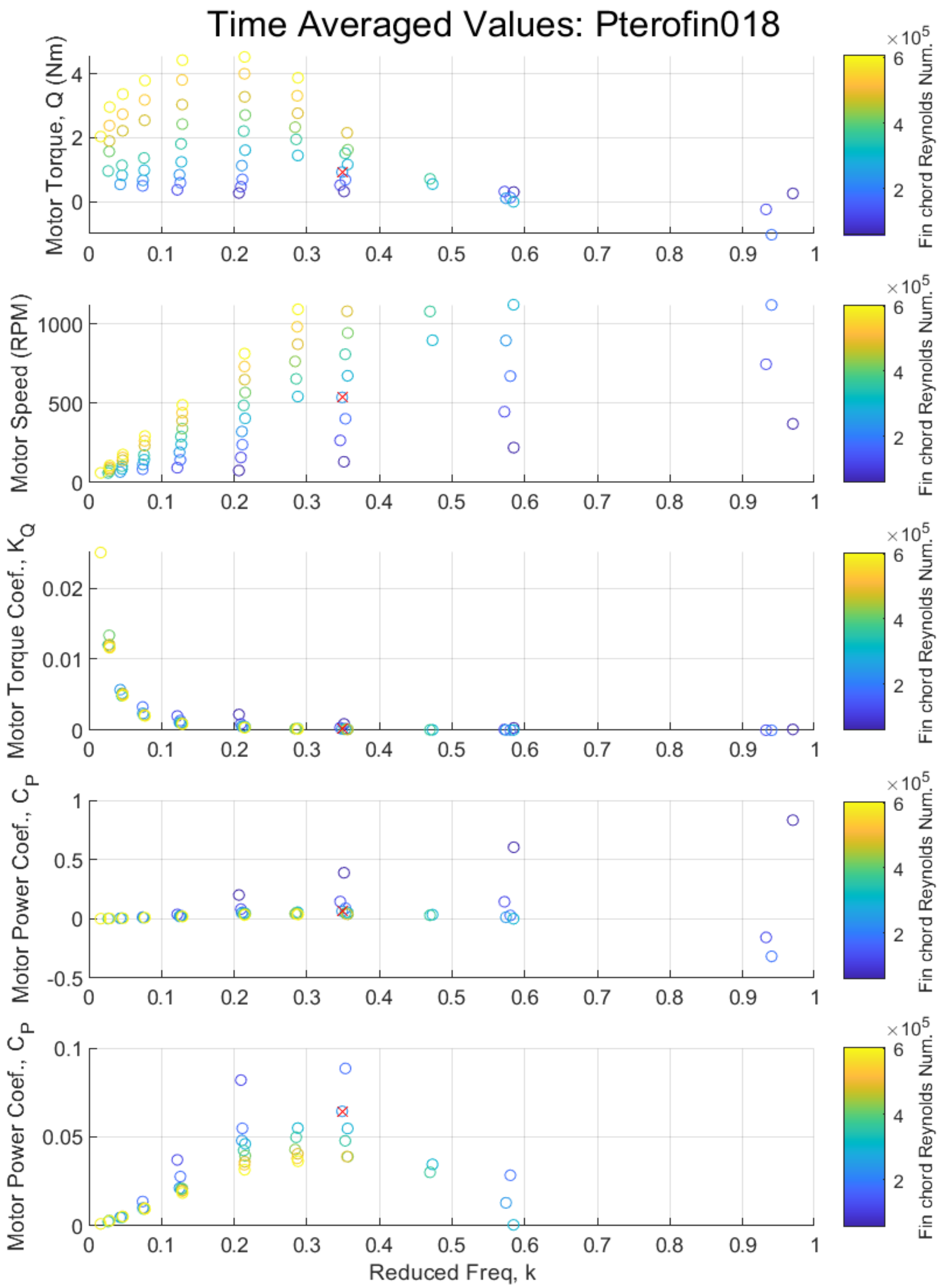
Time Averaged Values: Pterofin018
Motor Torque, Q (Nm)
Motor Speed (RPM)
Motor Torque Coef., K_Q
Motor Power Coef., C_P
Motor Power Coef., C_P
Reduced Freq, k
Fin chord Reynolds Num.
$\times 10^5$

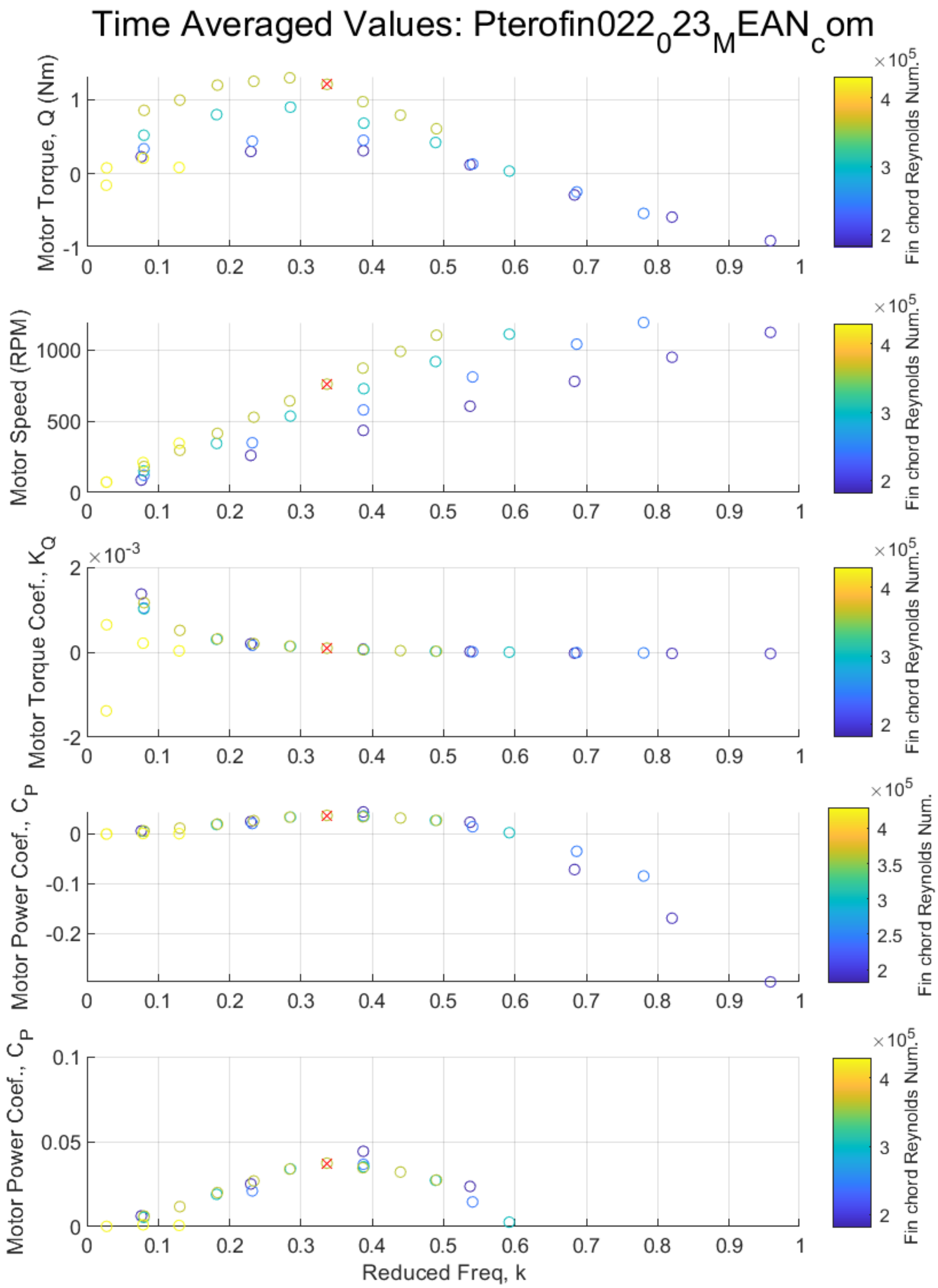
Time Averaged Values: Pterofin022_023_MEAN_com
Motor Torque, Q (Nm)
Motor Speed (RPM)
Motor Torque Coef., K_Q
×10^-3
Motor Power Coef., C_P
Motor Power Coef., C_P
Reduced Freq, k
Fin chord Reynolds Num.
×10^5
0
0.1
0.2
0.3
0.4
0.5
0.6
0.7
0.8
0.9
1

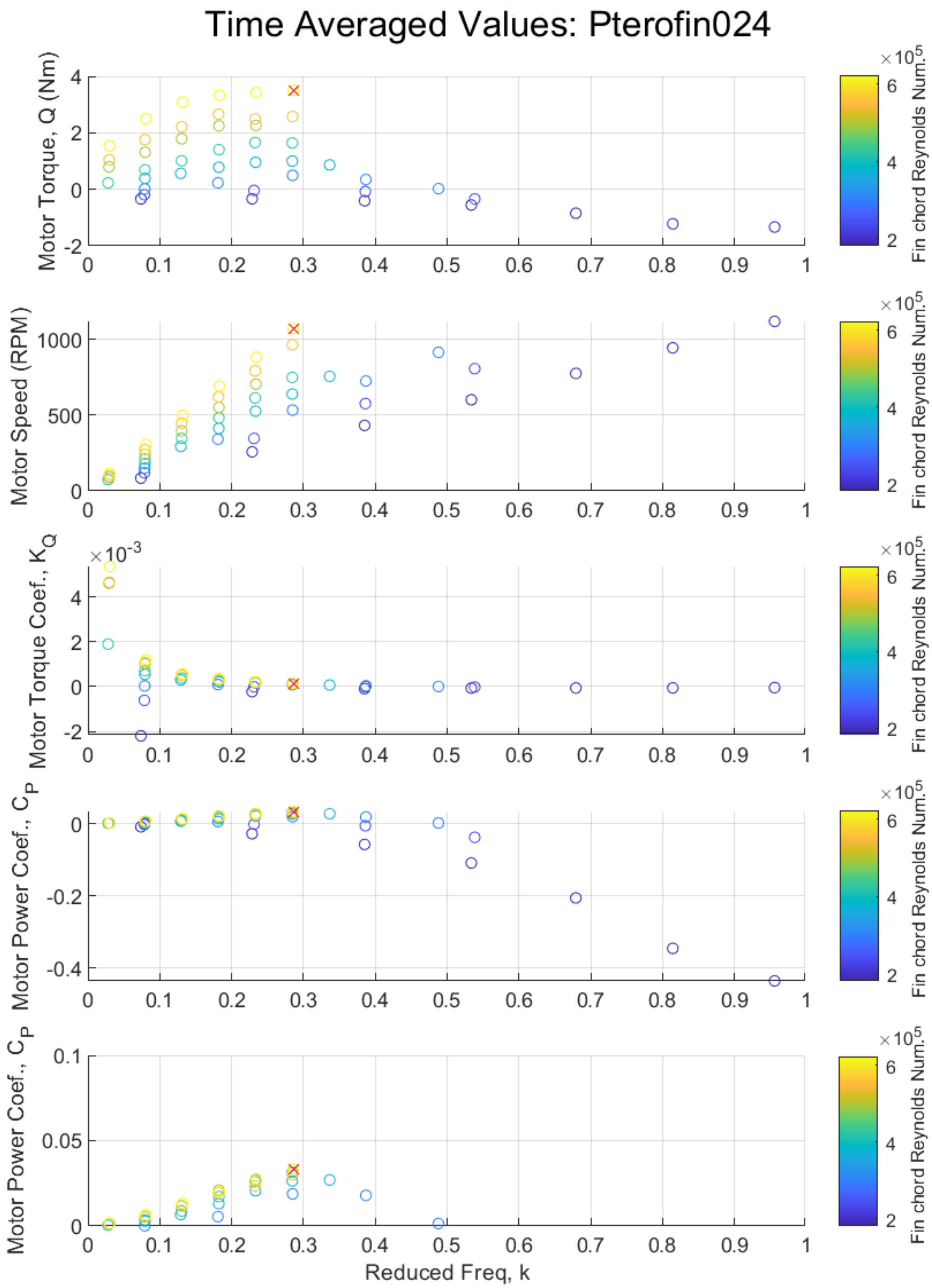
Time Averaged Values: Pterofin024
Motor Torque, Q (Nm)
Motor Speed (RPM)
Motor Torque Coef., K_Q
$\times10^{-3}$
Motor Power Coef., C_P
Motor Power Coef., C_P
Reduced Freq, k
Fin chord Reynolds Num.
$\times10^{5}$

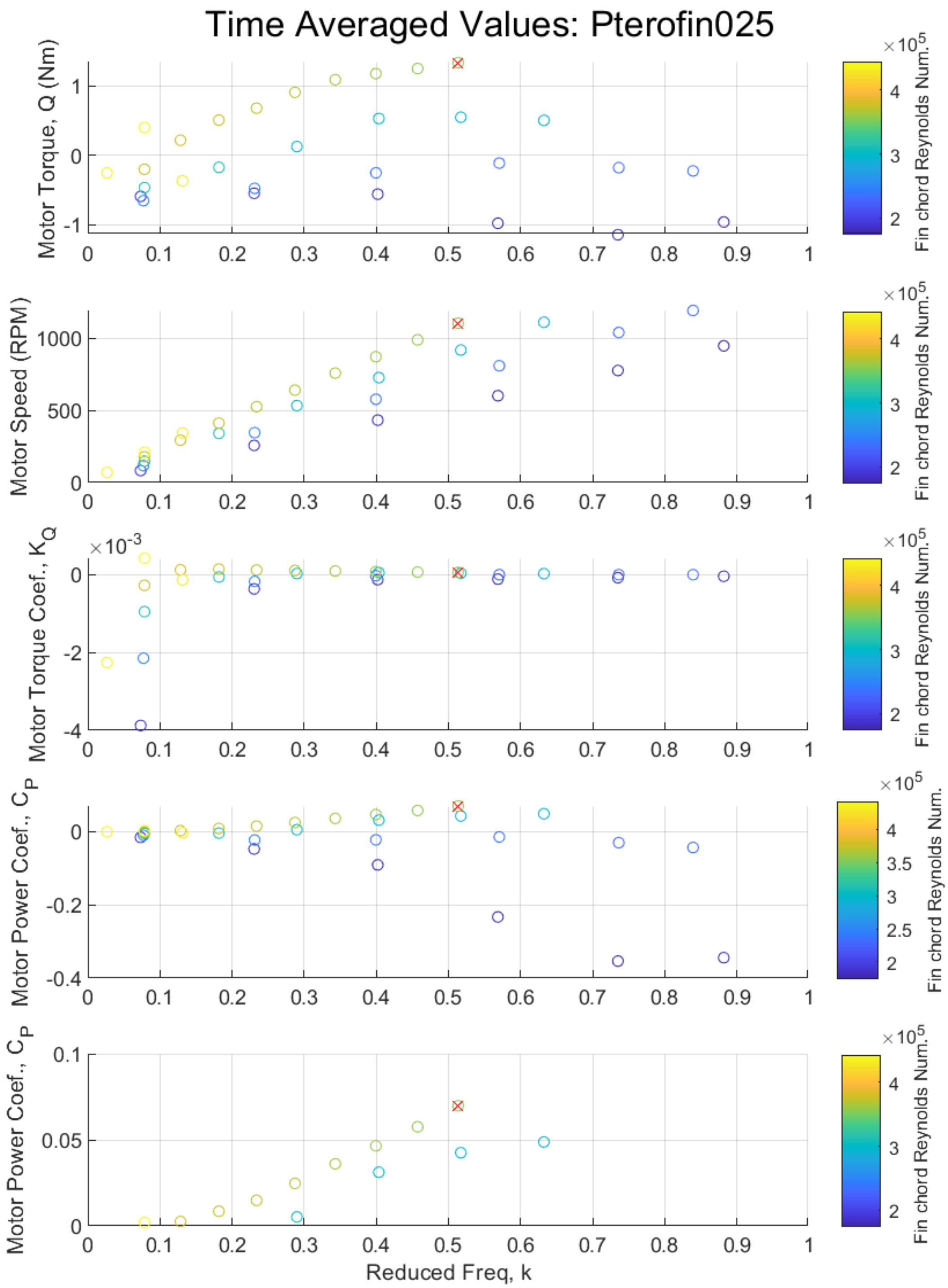
Time Averaged Values: Pterofin025
Motor Torque, Q (Nm)
Motor Speed (RPM)
Motor Torque Coef., K_Q
Motor Power Coef., C_P
Motor Power Coef., C_P
Reduced Freq, k
Fin chord Reynolds Num.
$\times 10^5$
$\times 10^{-3}$

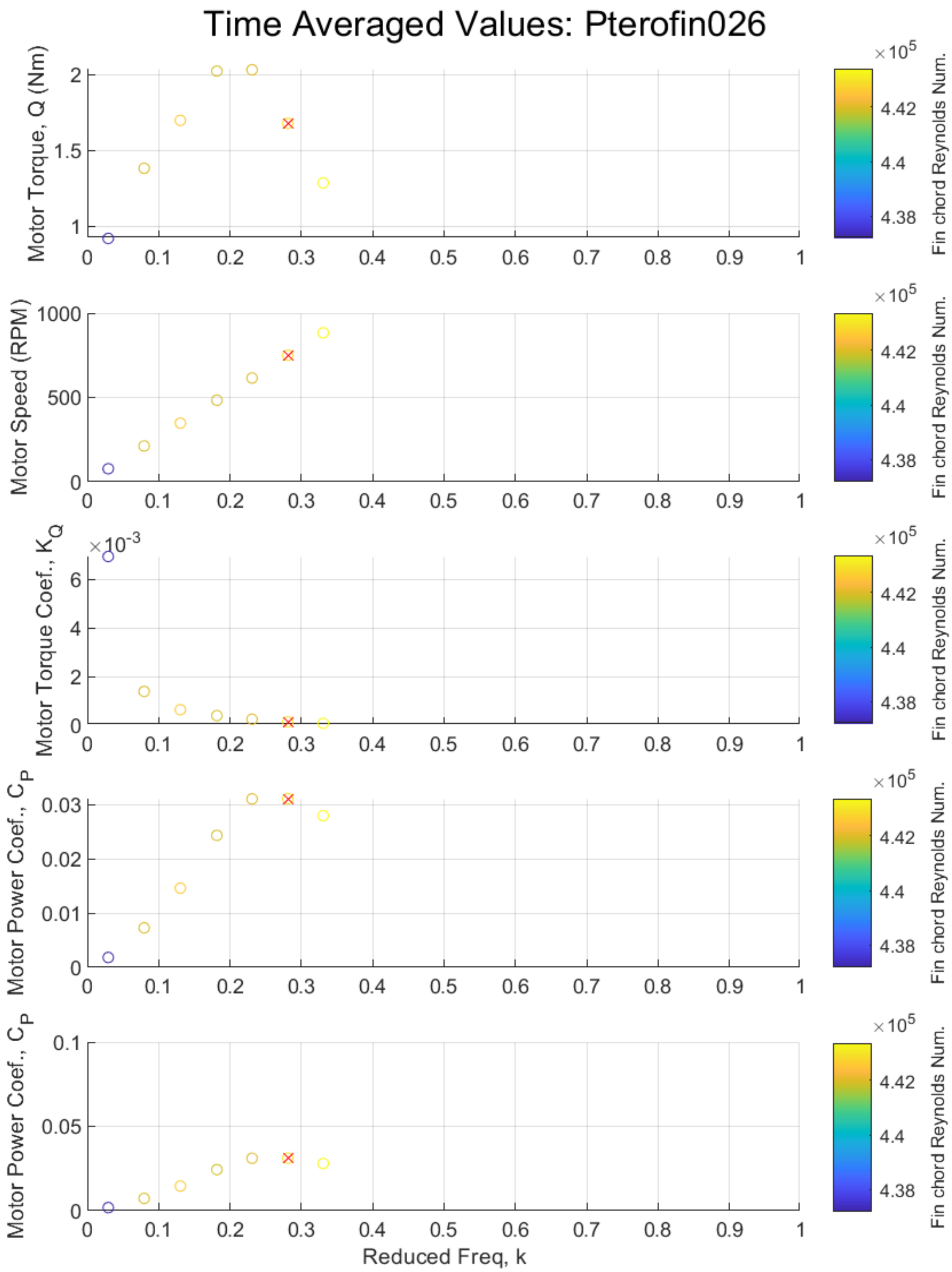
Time Averaged Values: Pterofin026
Motor Torque, Q (Nm)
Motor Speed (RPM)
Motor Torque Coef., K_Q
$\times 10^{-3}$
Motor Power Coef., C_P
Motor Power Coef., C_P
Reduced Freq, k
Fin chord Reynolds Num.
$\times 10^5$
4.42
4.4
4.38

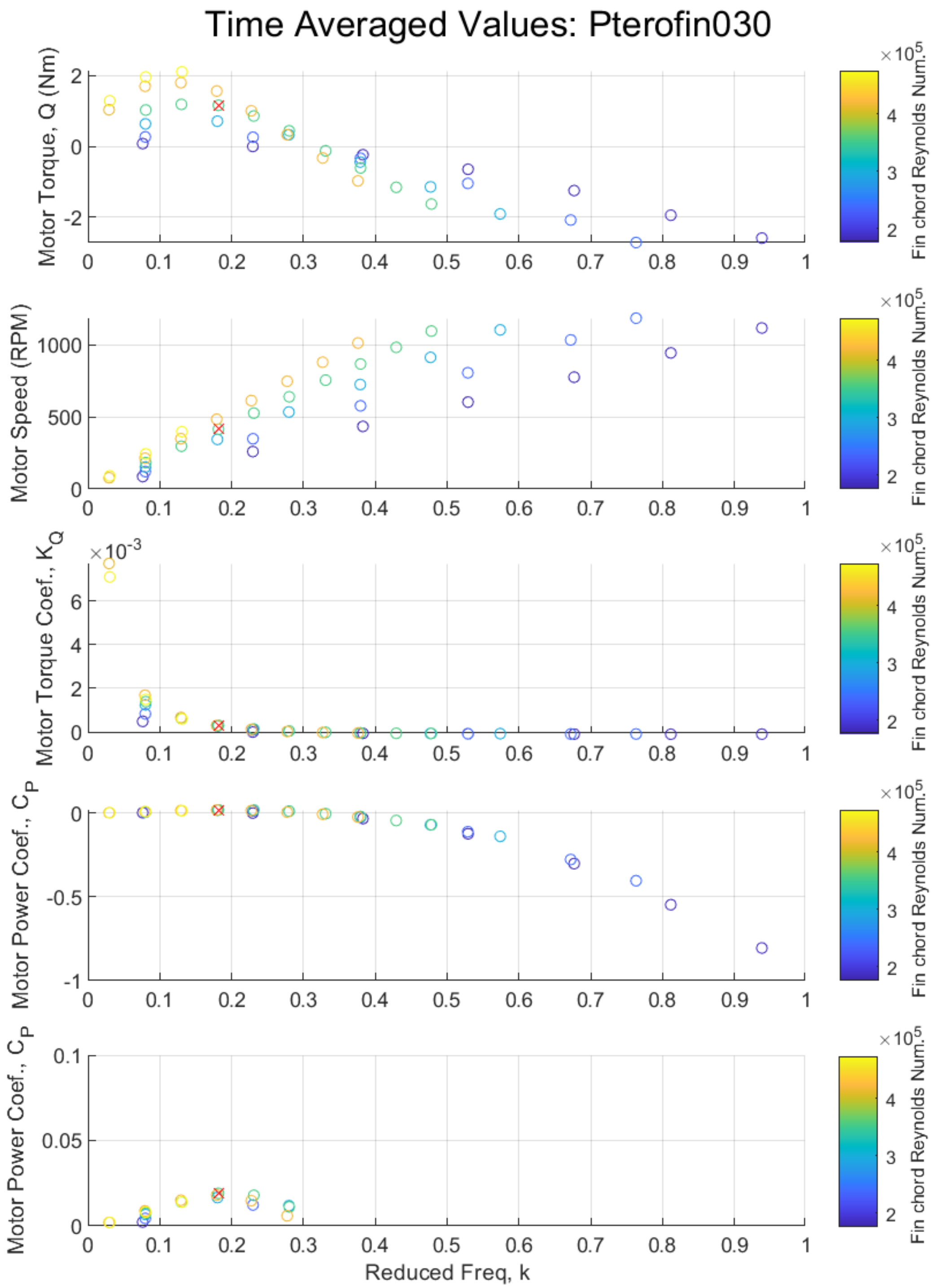
Time Averaged Values: Pterofin030
Motor Torque, Q (Nm)
Motor Speed (RPM)
Motor Torque Coef., K_Q
Motor Power Coef., C_P
Motor Power Coef., C_P
Reduced Freq, k
Fin chord Reynolds Num.
$\times 10^5$
$\times 10^{-3}$

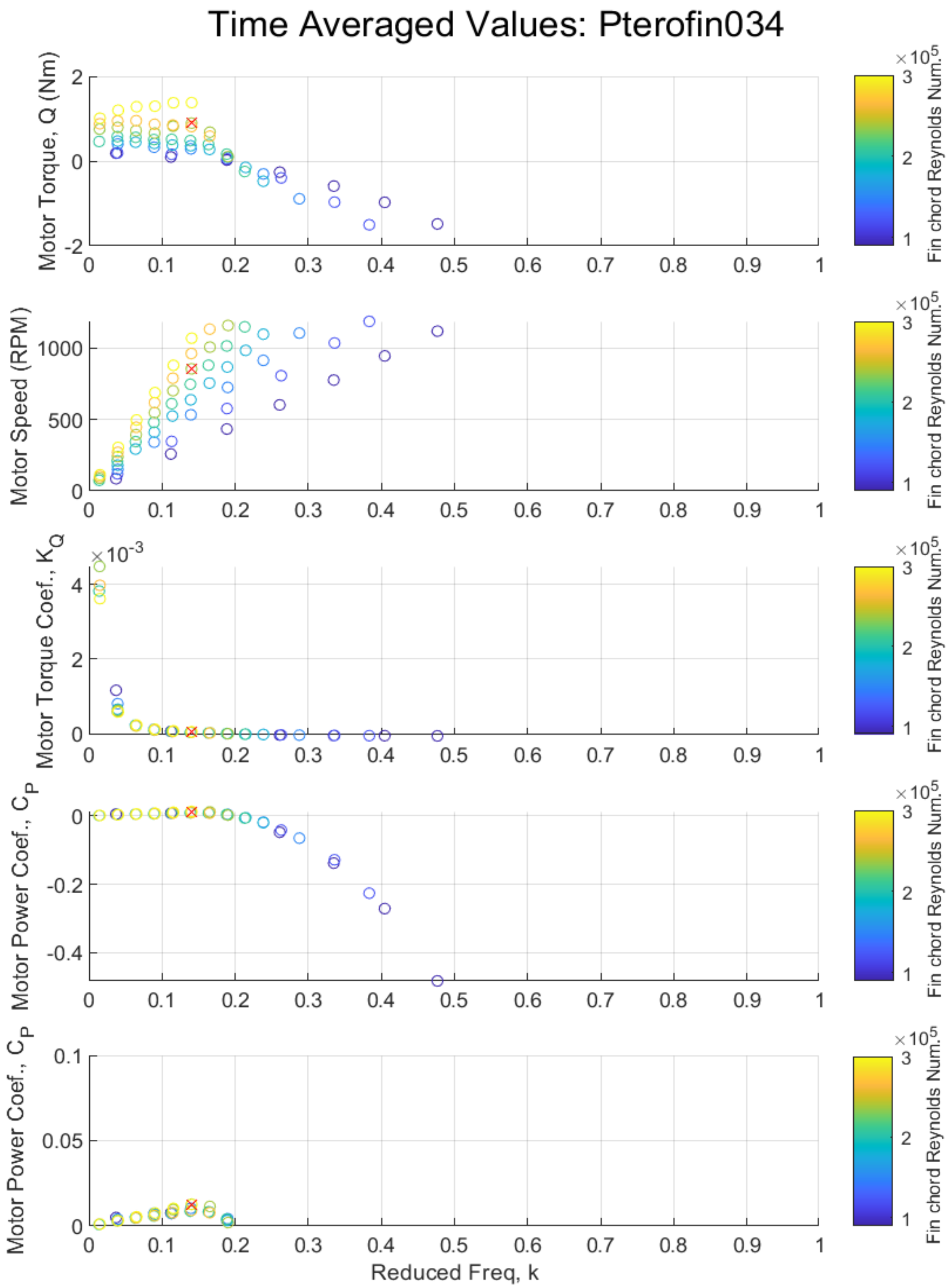
Time Averaged Values: Pterofin034
Motor Torque, Q (Nm)
Motor Speed (RPM)
Motor Torque Coef., K_Q
$\times 10^{-3}$
Motor Power Coef., C_P
Motor Power Coef., C_P
Reduced Freq, k
Fin chord Reynolds Num.
$\times 10^{5}$

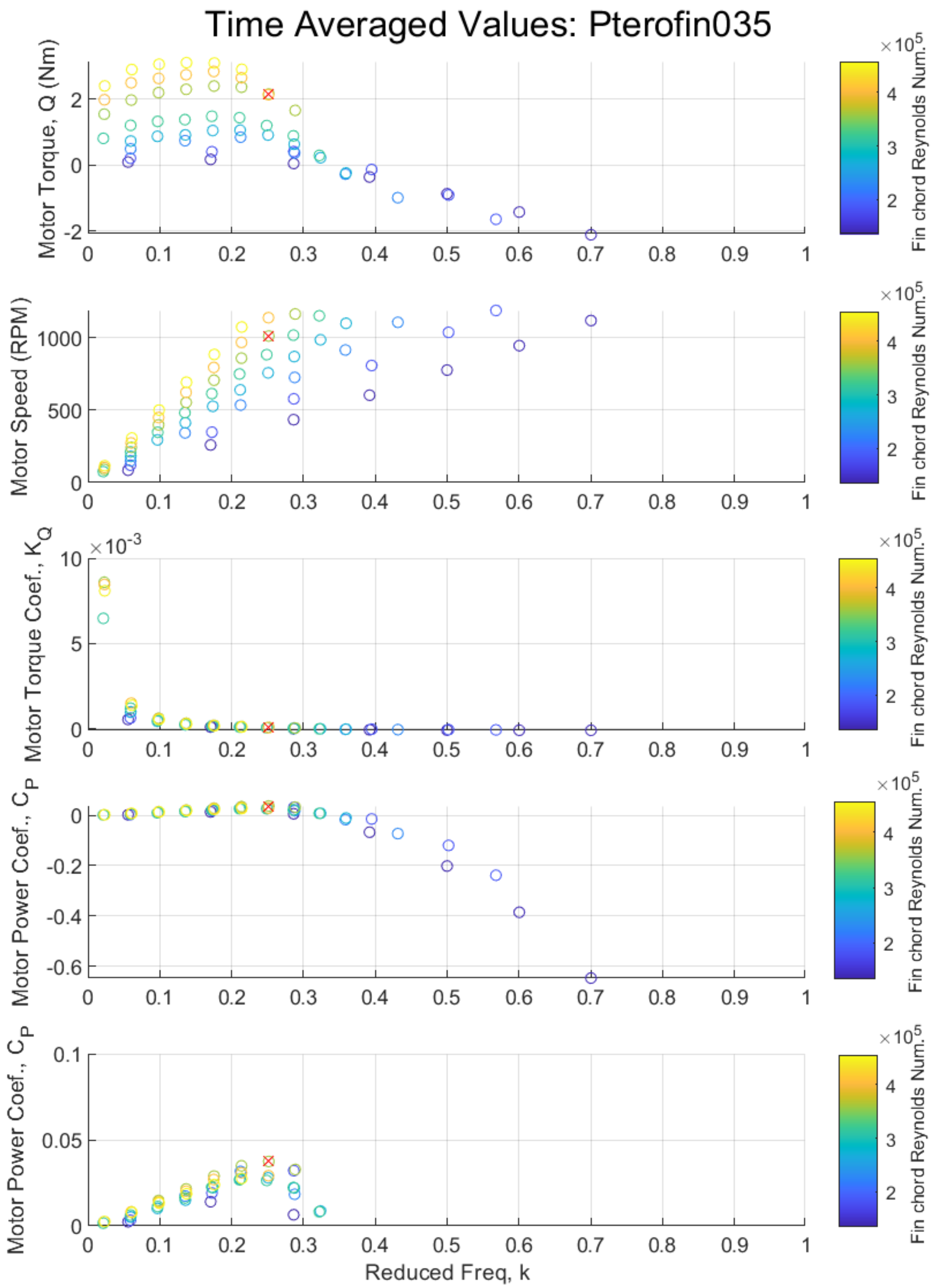

Time Averaged Values: Pterofin035
Motor Torque, Q (Nm)
Motor Speed (RPM)
Motor Torque Coef., K_Q
Motor Power Coef., C_P
Motor Power Coef., C_P
Reduced Freq, k
Fin chord Reynolds Num.
$\times 10^5$
$\times 10^{-3}$

Testing & Expertise for Marine Energy

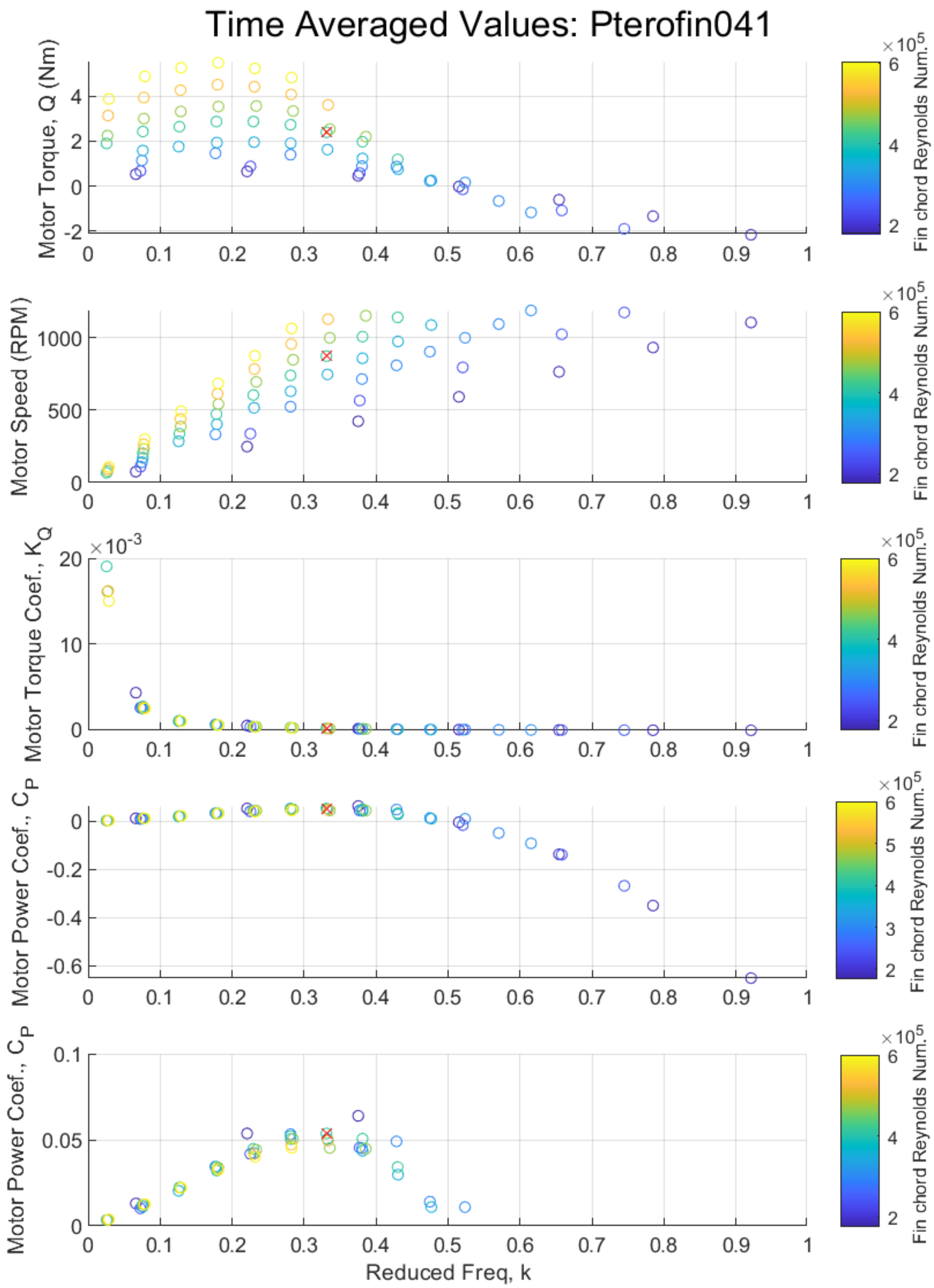

Appendix D - Processed Data: Phase Averaged Values

The following figures show the phase averaged values resulting from analysis of pre-processed test data. Each figure corresponds to one run from a test, which typically corresponds to a fin and mechanism configuration at a combination of mechanism and tunnel conditions (Reynolds number and reduced frequency). Generally speaking the runs selected for plotting are at relatively high Reynolds number and at a reduced frequency corresponding to maximum power coefficient within that test.

Wherever possible phase averaged measurements of interest (motor torque, motor RPM, freestream velocity) and system performance metrics (reduced frequency, power coefficient, and torque coefficient) can be found in comma separated variable files for each run in a folder structure corresponding to the date the test was conducted. For example, for run "Pterofin004R001" the pre-processed time series data can be found in the deliverable data file system, subfolder:

/2023/06/22/Pterofin0004/Pterofin004R001.csv

The phase averaged values derived from the pre-processed test data are located in the same folder, filename:

Pterofin004R001_PHASE_AVERAGED.csv

Each of the following figures includes plots of mean values, phase averaged values, and bounds of plus or minus two standard deviations from the phase averaged value.

Testing & Expertise for Marine Energy

Phase Statistics: Pterofin004R043

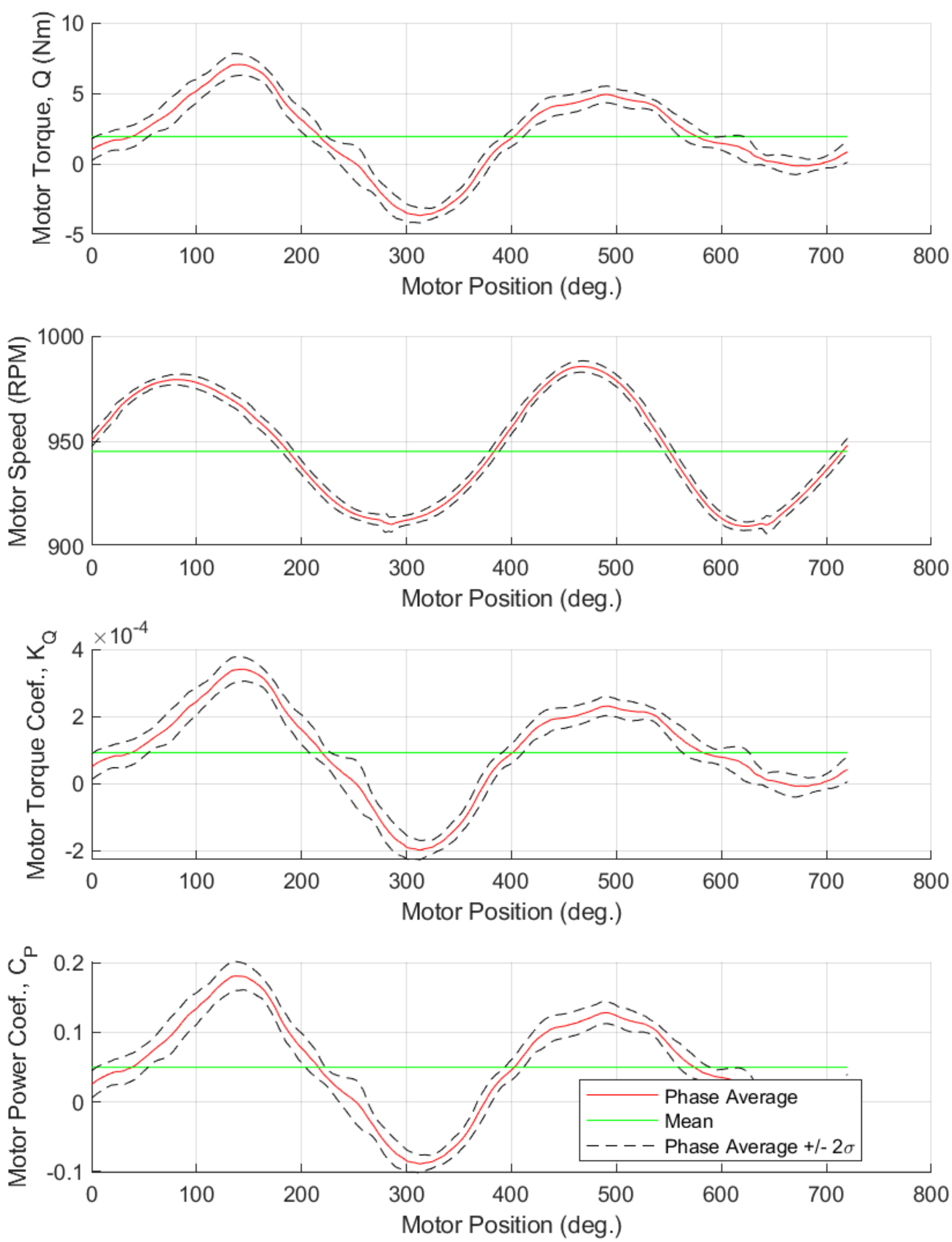

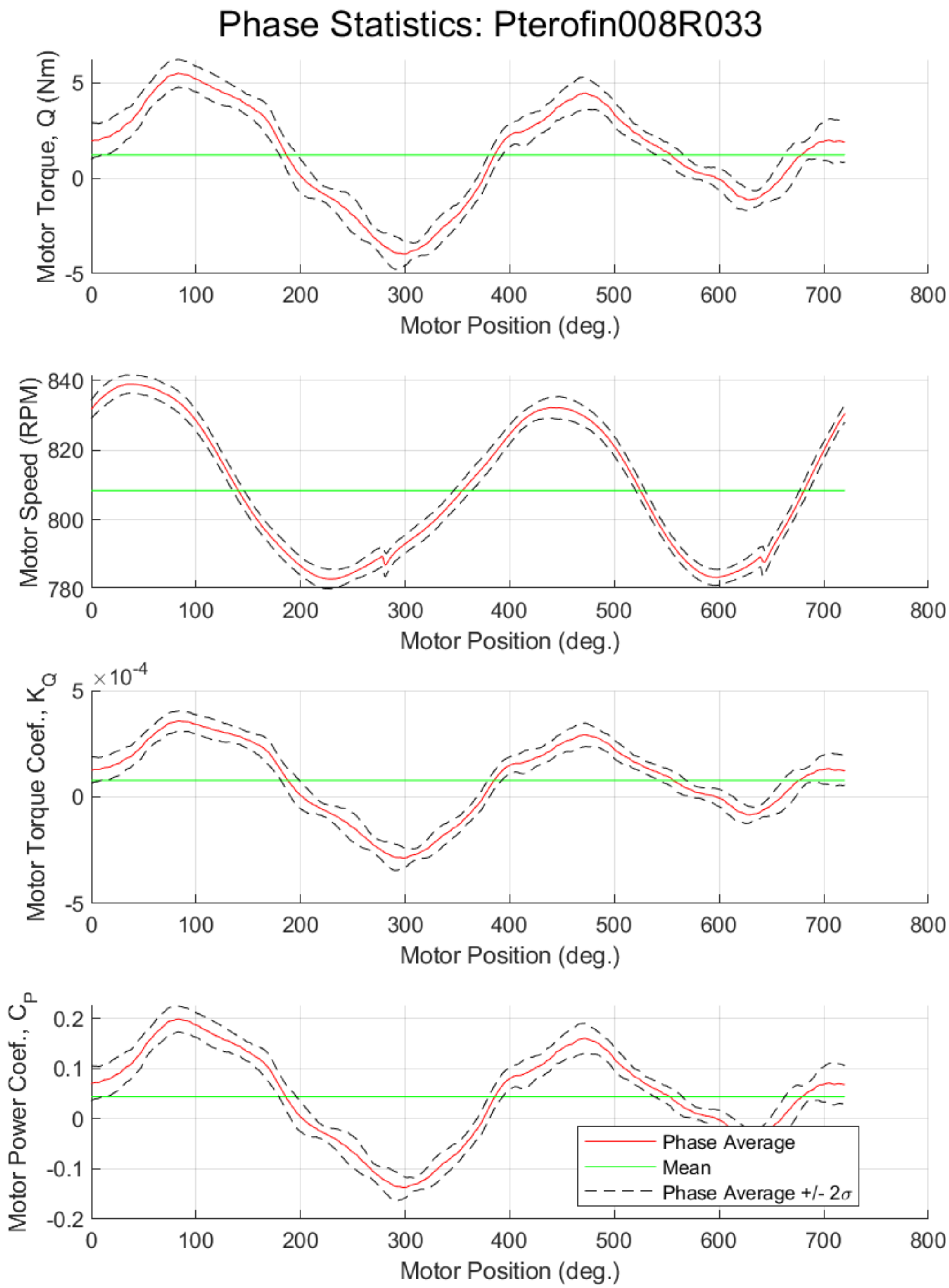
Phase Statistics: Pterofin008R033
Motor Torque, Q (Nm)
Motor Position (deg.)
Motor Speed (RPM)
Motor Position (deg.)
Motor Torque Coef., K_Q
$\times 10^{-4}$
Motor Position (deg.)
Motor Power Coef., C_P
Motor Position (deg.)
Phase Average
Mean
Phase Average +/- 2σ

Testing & Expertise for Marine Energy

Phase Statistics: Pterofin012R045

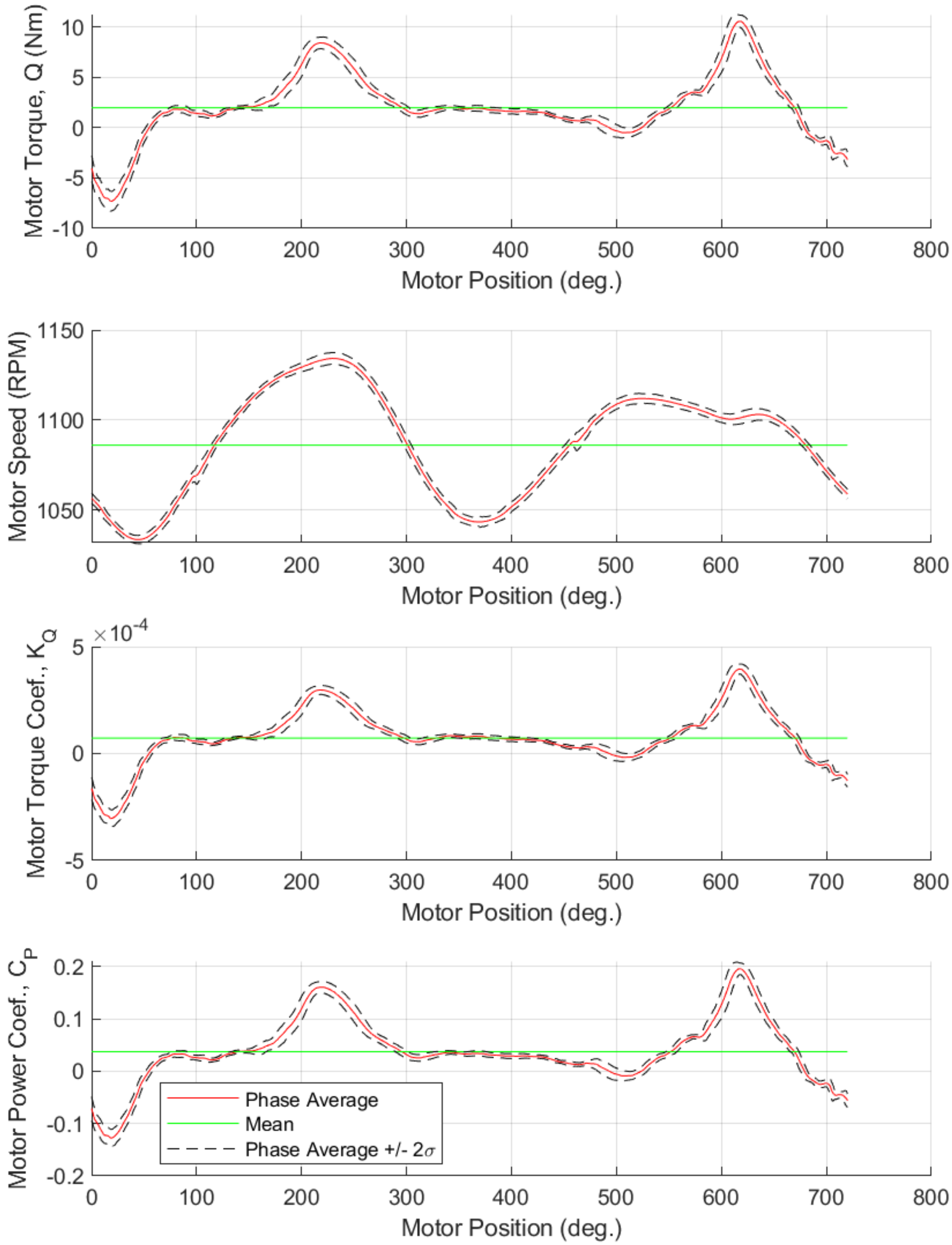

Phase Statistics: Pterofin014R045

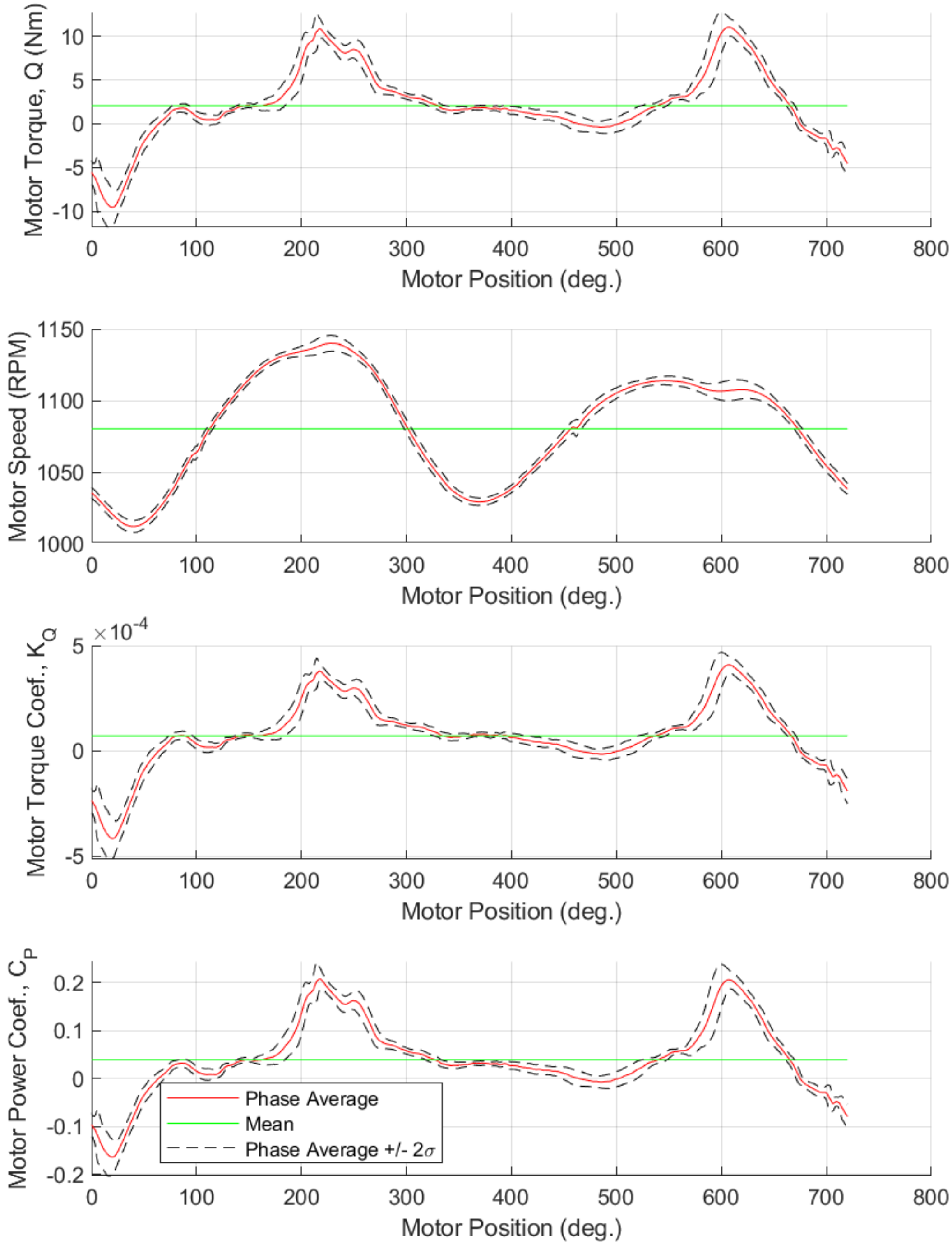

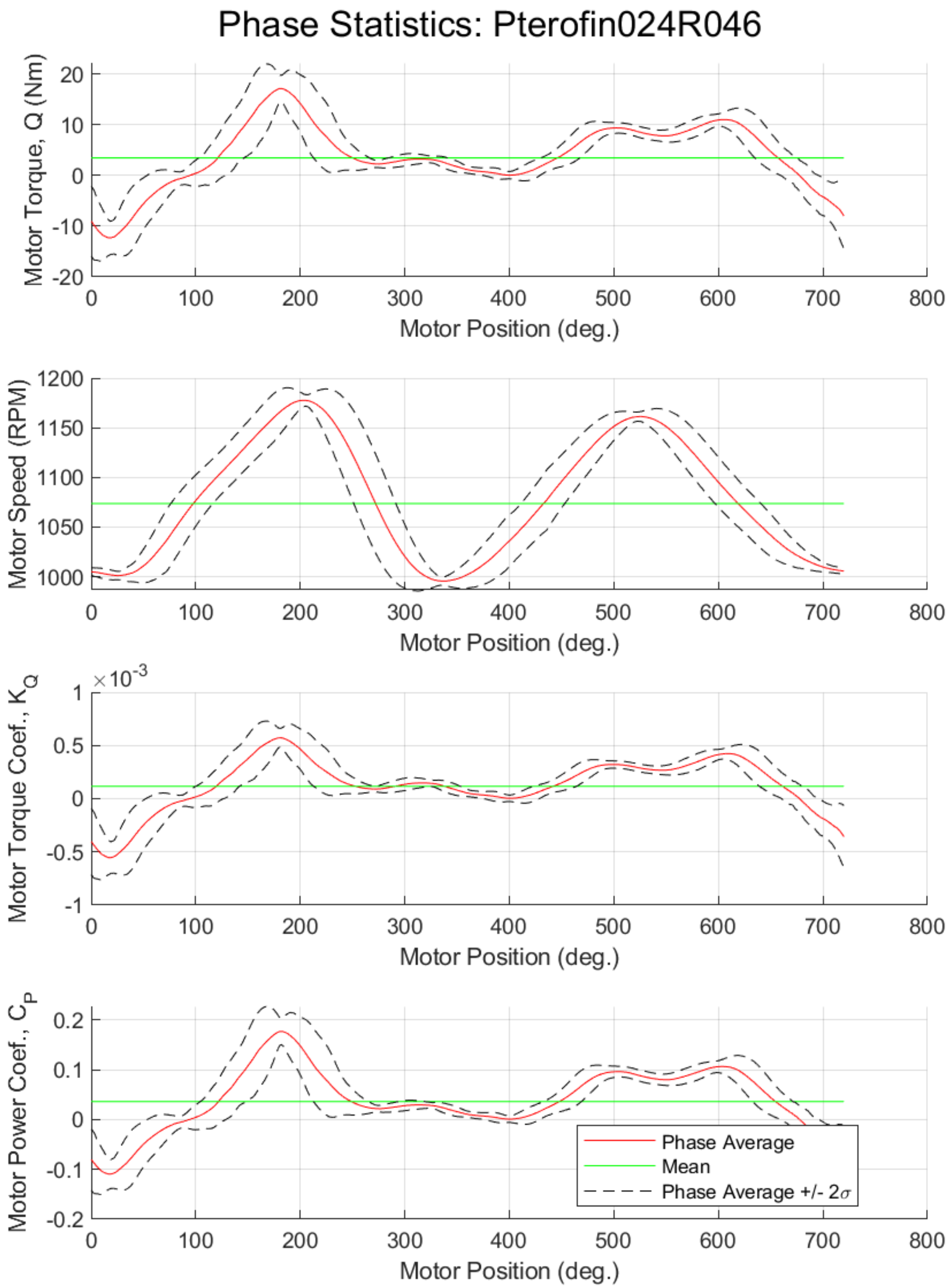
Phase Statistics: Pterofin024R046
Motor Torque, Q (Nm)
Motor Position (deg.)
Motor Speed (RPM)
Motor Position (deg.)
Motor Torque Coef., K_Q
$\times 10^{-3}$
Motor Position (deg.)
Motor Power Coef., C_P
Motor Position (deg.)
Phase Average
Mean
Phase Average +/- 2σ

Phase Statistics: Pterofin025R029

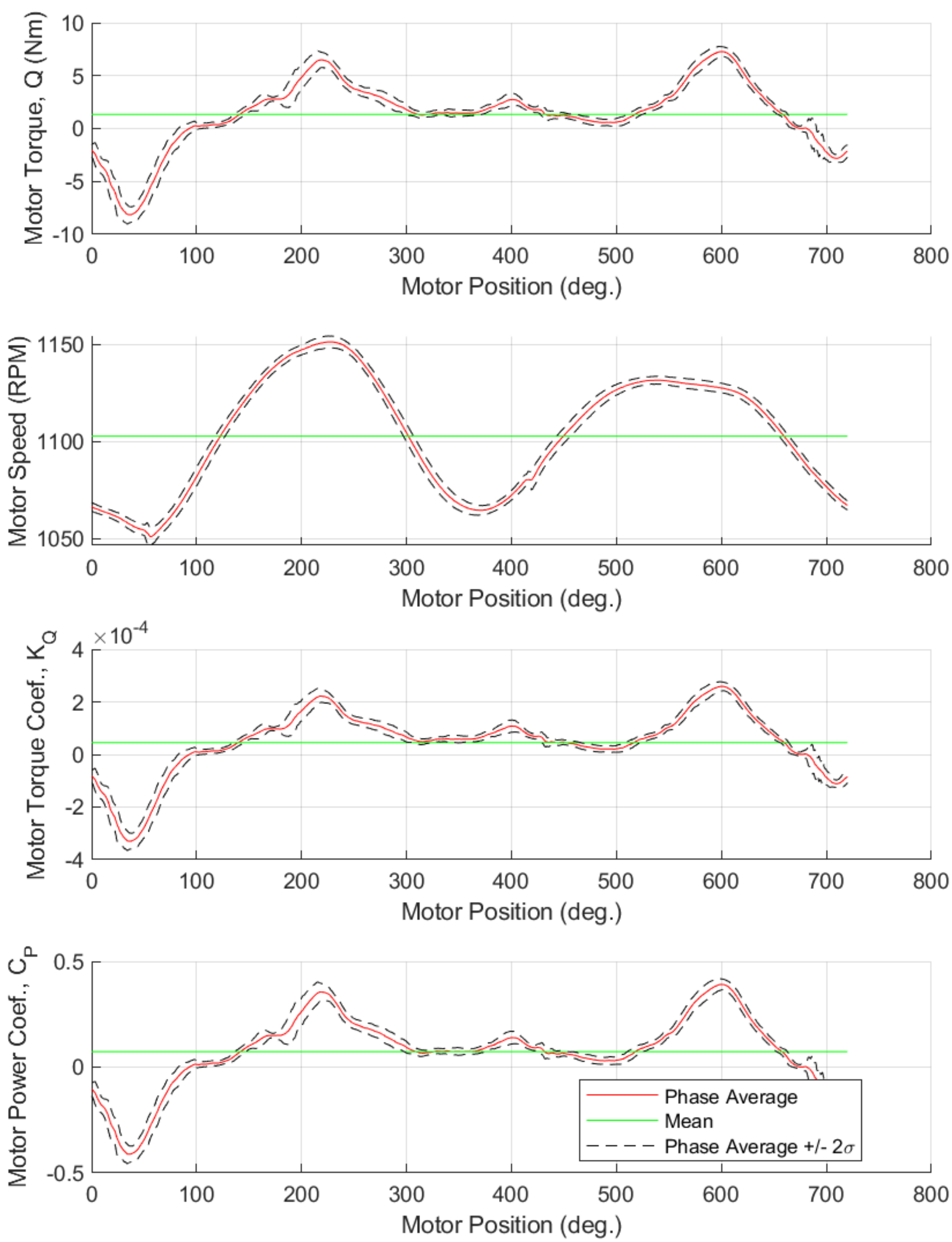

Phase Statistics: Pterofin030R023

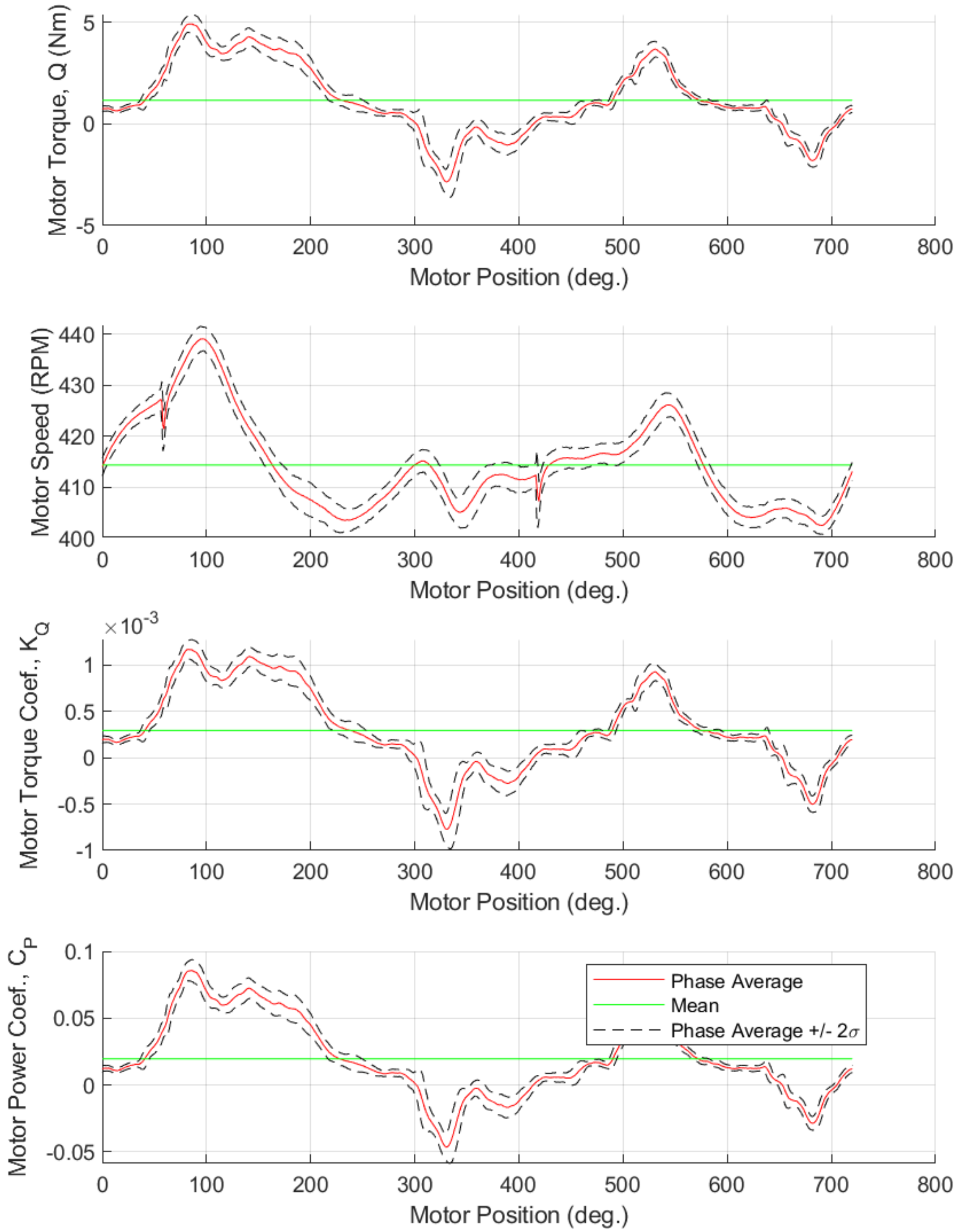

Phase Statistics: Pterofin034R059

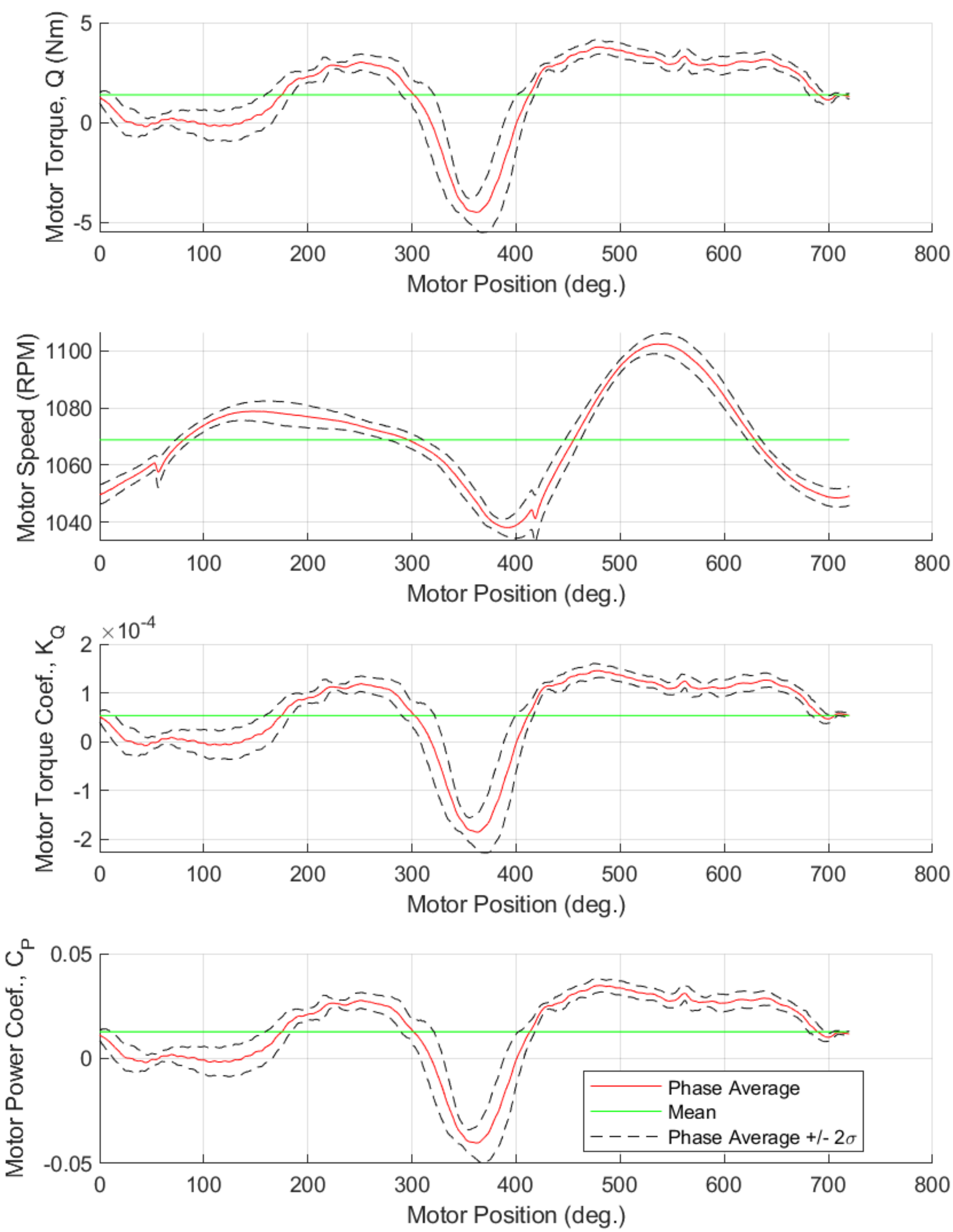

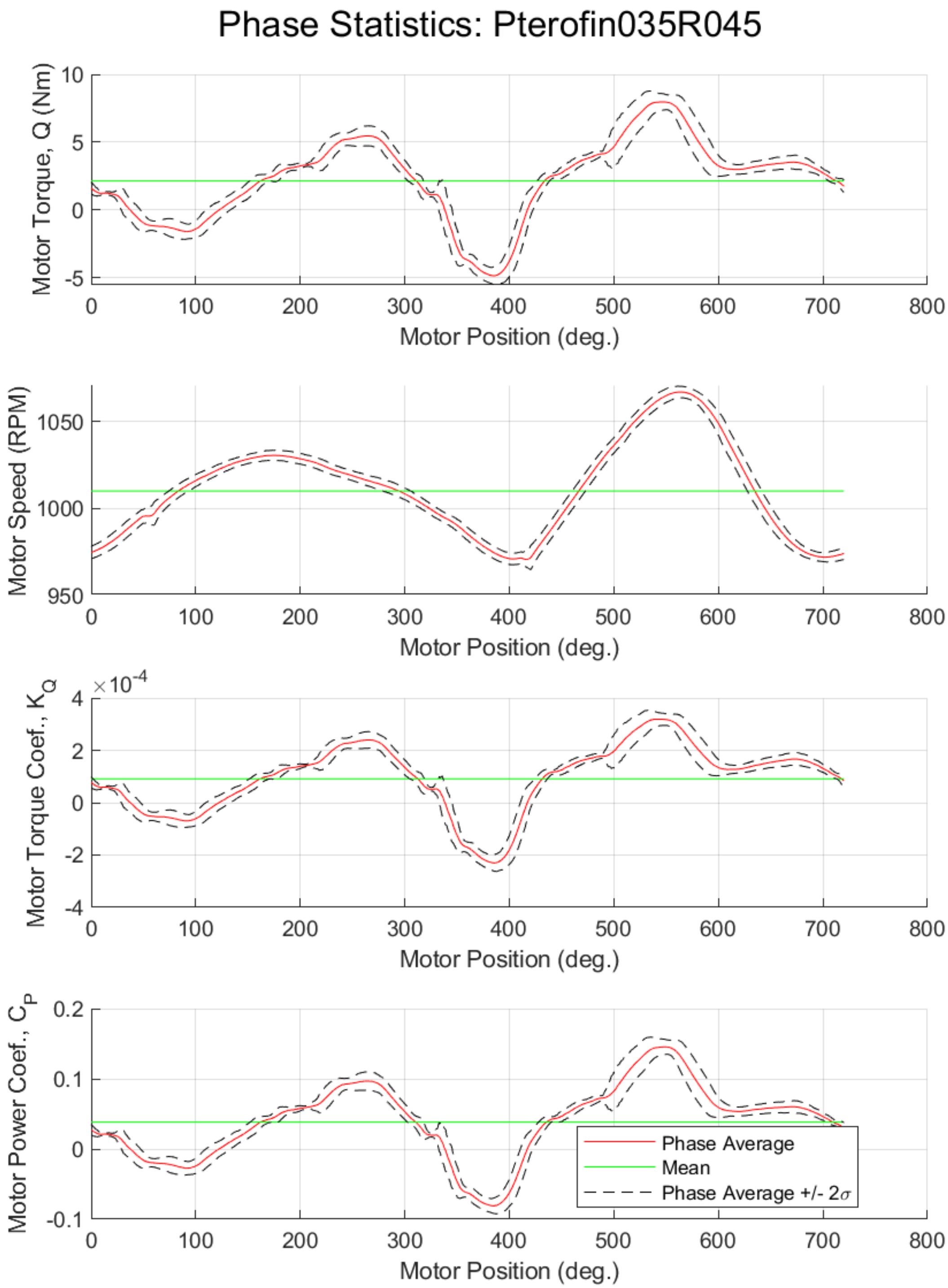
Phase Statistics: Pterofin035R045
Motor Torque, Q (Nm)
Motor Position (deg.)
Motor Speed (RPM)
Motor Position (deg.)
Motor Torque Coef., K_Q
$\times 10^{-4}$
Motor Position (deg.)
Motor Power Coef., C_P
Motor Position (deg.)
Phase Average
Mean
Phase Average +/- 2σ

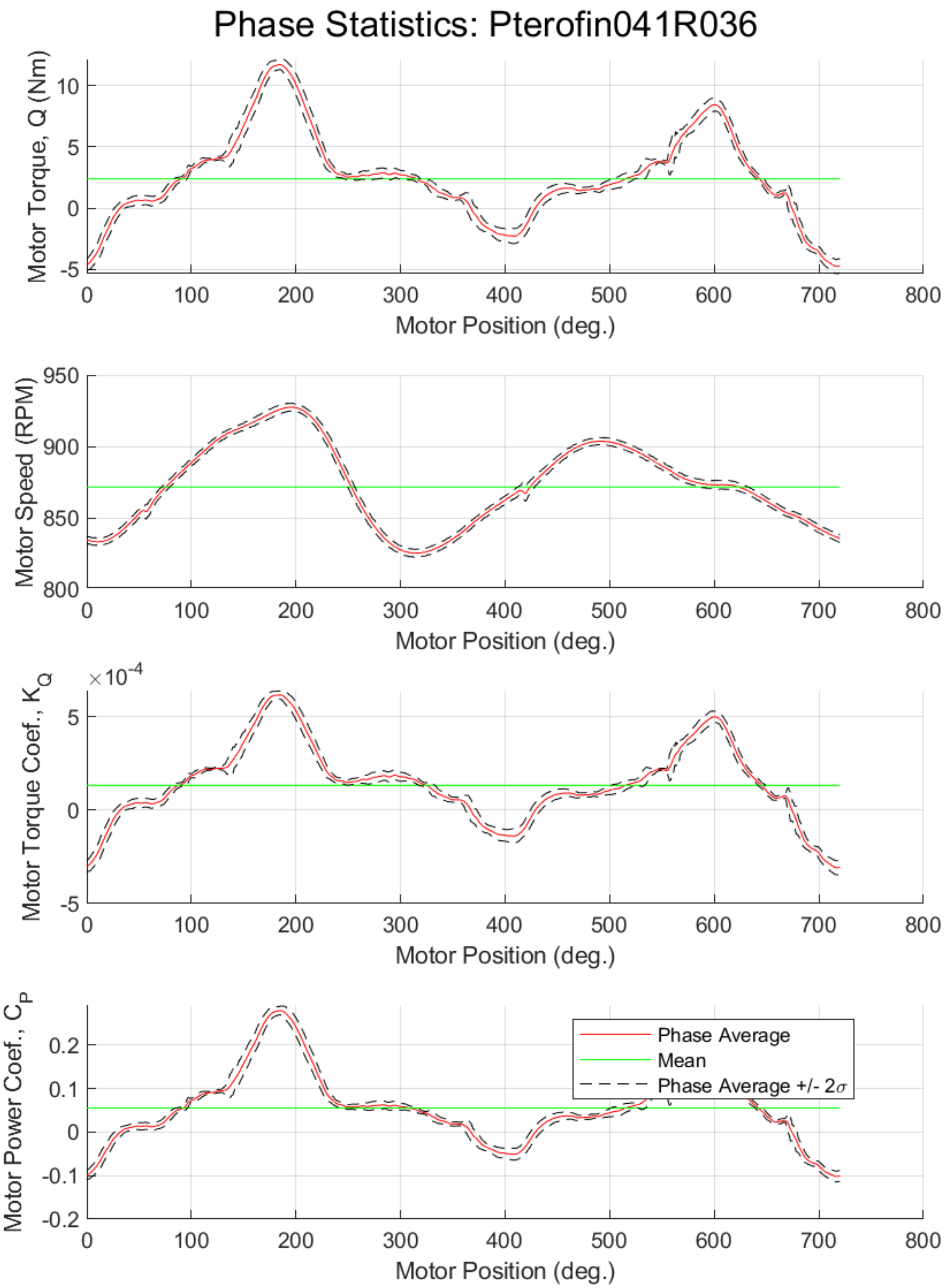
Phase Statistics: Pterofin041R036
Motor Torque, Q (Nm)
Motor Position (deg.)
Motor Speed (RPM)
Motor Position (deg.)
Motor Torque Coef., K_Q
×10^-4
Motor Position (deg.)
Motor Power Coef., C_P
Phase Average
Mean
Phase Average +/- 2σ
Motor Position (deg.)